Flow Perturbation Mediates Neutrophil Recruitment and Potentiates Endothelial Injury via TLR2 in Mice

Implications for Superficial Erosion

Grégory Franck, Thomas Mawson, Grasiele Sausen, Manuel Salinas, Gustavo Santos Masson, Andrew Cole, Marina Beltrami-Moreira, Yiannis Chatzizisis, Thibault Quillard, Yevgenia Tesmenitsky, Eugenia Shvartz, Galina K. Sukhova, Filip K. Swirski, Matthias Nahrendorf, Elena Aikawa, Kevin J. Croce, Peter Libby

Rationale: **Superficial erosion currently causes up to a third of acute coronary syndromes; yet, we lack understanding of its mechanisms. Thrombi because of superficial intimal erosion characteristically complicate matrix-rich atheromata in regions of flow perturbation.**

Objective: **This study tested in vivo the involvement of disturbed flow and of neutrophils, hyaluronan, and Toll-like receptor 2 ligation in superficial intimal injury, a process implicated in superficial erosion.**

Methods and Results: **In mouse carotid arteries with established intimal lesions tailored to resemble the substrate of human eroded plaques, acute flow perturbation promoted downstream endothelial cell activation, neutrophil accumulation, endothelial cell death and desquamation, and mural thrombosis. Neutrophil loss-of-function limited these findings. Toll-like receptor 2 agonism activated luminal endothelial cells, and deficiency of this innate immune receptor decreased intimal neutrophil adherence in regions of local flow disturbance, reducing endothelial cell injury and local thrombosis ($P<0.05$).**

Conclusions: **These results implicate flow disturbance, neutrophils, and Toll-like receptor 2 signaling as mechanisms that contribute to superficial erosion, a cause of acute coronary syndrome of likely growing importance in the statin era. (*Circ Res*. 2017;121:31-42. DOI: 10.1161/CIRCRESAHA.117.310694.)**

Key Words: acute coronary syndromes ■ disturbed flow ■ endothelium ■ neutrophils ■ superficial erosion

Rupture of an atheromatous plaque with a thin fibrous cap has received much attention as a cause of acute coronary syndrome (ACS).[1,2] Abundant human and experimental findings indicate that lipid lowering, in particular statin treatment, mitigates this mechanism of plaque disruption.[3] Current clinical data show a shift in the characteristics of plaques associated with rupture (lipid and macrophage rich), concomitant with increased statin use, smoking cessation, and other reductions in risk factors. Human atheromata today contain less lipid and fewer macrophages than just a decade ago.[4,5] But even with the best current medical and interventional therapy, the residual burden of recurrent events post-ACS remains unacceptable.[6] Indeed, ruptured thin-capped atheromata may now cause fewer ACS,[7] and superficial erosion appears on the rise. Yet, mechanisms involved in superficial erosion have received scant attention and remain a major knowledge gap.

Editorial, see p 8
In This Issue, see p 2
Meet the First Author, see p 3

Thrombi associated with superficial erosion generally overlie fibrous rather than lipid-rich plaques. In contrast to plaques with ruptured fibrous caps, eroded plaques contain few macrophages but abundant smooth muscle cells (SMCs). In stark contrast with collagen-poor ruptured plaques, eroded atheromata characteristically contain abundant type III collagen,[8,9] glycosaminoglycans, and proteoglycans.[10] Eroded plaques may localize preferentially in regions of low shear stress and exhibit impaired endothelial antithrombotic and atheroprotective functions[11–13] and loss of endothelial cell (EC).[14,15] Markers of EC apoptosis increase downstream of obstructive atherosclerotic plaques in humans, sites of disturbed flow.[16] Oscillatory wall shear stress (WSS) favors EC

Original received January 24, 2017; revision received April 10, 2017; accepted April 20, 2017. In March 2017, the average time from submission to first decision for all original research papers submitted to *Circulation Research* was 15.11 days.

From the Department of Cardiovascular Medicine (G.F., T.M., G.S., M.S., A.C., M.B.-M., Y.C., T.Q., Y.T., E.S., G.K.S., E.A., K.J.C., P.L.), and Center for Interdisciplinary Cardiovascular Sciences (E.A.), Brigham and Women's Hospital, Harvard Medical School, Boston, MA; Center for Systems Biology, Massachusetts General Hospital, Harvard Medical School, Boston (G.S.M., F.K.S., M.N.); and Department of Engineering and Technology, College of Engineering and Computing, Nova Southeastern University, Fort Lauderdale, FL (M.S.).

The online-only Data Supplement is available with this article at http://circres.ahajournals.org/lookup/suppl/doi:10.1161/CIRCRESAHA.117.310694/-/DC1.

Correspondence to Peter Libby, MD, Cardiovascular Medicine, Brigham and Women's Hospital, Harvard Medical School, Boston, MA 02115. E-mail plibby@bwh.harvard.edu

Novelty and Significance

What Is Known?

- Superficial erosion involves discontinuity in the intimal endothelium and thrombus formation without plaque rupture.
- Erosion-prone plaques have specific features and associate with the presence of neutrophils.

What New Information Does This Article Contribute?

- Validation of an in vivo approach to recapitulate aspects of superficial erosion in mice to permit mechanistic explorations.
- A demonstration that neutrophils contribute critically to arterial endothelial cell injury in regions of disturbed arterial flow.
- Establishing a role for endothelial Toll-like receptor 2 in local neutrophil recruitment.

Postmortem pathological studies demonstrated the loss of endothelial cells at sites of superficial erosion of the culprit lesions of acute coronary syndromes; yet, the mechanisms that drive this process remain elusive. We developed a new in vivo approach in mice that involves creating a chronic intimal lesion that recapitulates certain features associated with superficial erosion, followed by introduction of flow disturbance. We found that neutrophils selectively accumulate in the lumen of carotid arteries under these circumstances. This neutrophil recruitment locally disrupted the endothelial layer. Toll-like receptor 2 loss of function in arterial but not in bone marrow–derived cells blunted these effects. These findings illustrate the utility of a novel experimental tool to study the mechanisms of arterial thrombi in the absence of plaque rupture.

Nonstandard Abbreviations and Acronyms

ACS	acute coronary syndrome
ApoE	apolipoprotein E
CC	constrictive cuff
CXCL	chemokine (C-X-C motif) ligand
EC	endothelial cell
HA	hyaluronic acid/hyaluronan
LCCA	left common carotid artery
MPO	myeloperoxidase
NC	Nonconstrictive cuff
NETs	neutrophil extracellular traps
Pam3	Pam3CSK4
SMC	smooth muscle cell
TLR2	Toll like receptor 2
VCAM-1	vascular cell adhesion molecule 1
WSS	wall shear stress

death[17–19] in stenotic arteries with expanded intimas in rabbits, promoting thrombosis.[20] EC apoptosis activates thrombin and platelet adhesion in vitro,[21,22] as well as local EC desquamation and thrombosis in vivo.[23]

Zones of flow perturbation have high EC Toll-like receptor 2 (TLR2) expression in mouse and human atheromata,[24,25] and loss of TLR2 function limits murine atherogenesis.[26] Hyaluronan (HA), a glycosaminoglycan prominent in human eroded plaques can ligate TLR2.[10,27] We and others recently provided in vitro data supporting the involvement of TLR2 and HA in EC activation[28] associated with the release of the neutrophil chemoattractant interleukin-8 and augmented leukocyte adhesion molecules (eg, vascular cell adhesion molecule 1 [VCAM-1] and E-selectin). TLR2 expression further correlates with the number of apoptotic luminal ECs in human plaques with characteristics of superficial erosion and with neutrophils and neutrophil extracellular traps (NETs).[28] Patients with ACS because of superficial erosion (versus rupture) have higher concentrations of circulating myeloperoxidase,[29] a neutrophil enzyme linked with EC death and tissue factor expression.[30] Interaction with neutrophils alters many functions of cultured EC.[28,31]

Thus, flow perturbation may comprise a first hit leading to chronic endothelial activation, propensity to slough, and impaired ability to repair small intimal breaches, setting the stage for an enhanced response to a second hit, such as local recruitment of neutrophils, able to augment EC apoptosis and propagate desquamation.[28] Such unrepaired rents in the endothelial monolayer could then trigger platelet entrapment, activation, and thrombin generation, fostering clot formation. These hypotheses, derived from in vitro observations, require exploration in vivo because cell culture experiments cannot fully mimic either the flow conditions or the abnormal intimal substrate associated with human superficial erosion.

Methods

See Methods in the Online Data Supplement.

Results

Thrombi caused by superficial erosion typically complicate plaques rich in HA, collagen, and SMC, but with scant macrophages, often located at sites of human coronary arteries surrounding stenoses, regions of disturbed flow. We sought clues regarding the mechanisms which might participate in endothelial loss in humans through study of atheromata harvested at carotid artery surgery. We used morphological criteria to classify different categories of plaques from specimens in our collection with well-preserved intimal surfaces (Figure 1). A group of plaques with a fibrous SMC-rich and macrophage-poor appearance was further subdivided into those with an erosion-prone morphology (high apoptotic EC content, n=7) or a stable fibrous morphology (low apoptotic EC content, n=10). A third group of fibrous plaques harbored a nonobstructive mural thrombus (eroded morphology, n=8; Online Figure IA). We compared these fibrous lesions to a group of atheromata with features associated with fibrous cap rupture: few SMC, many macrophages, and large lipid cores (n=11). Fibrous plaques with many apoptotic EC or those with mural thrombi displayed much greater accumulation of neutrophils near the luminal endothelium than those with few apoptotic EC (stable fibrous) or the thin-capped lipid- and macrophage-laden lesions (Figure 1A through 1D). Mural thrombi contained abundant neutrophils ($CD66b^+$ and neutrophil elastase $[NE]^+$; Figure 1C and 1D) as previously described.[32] In

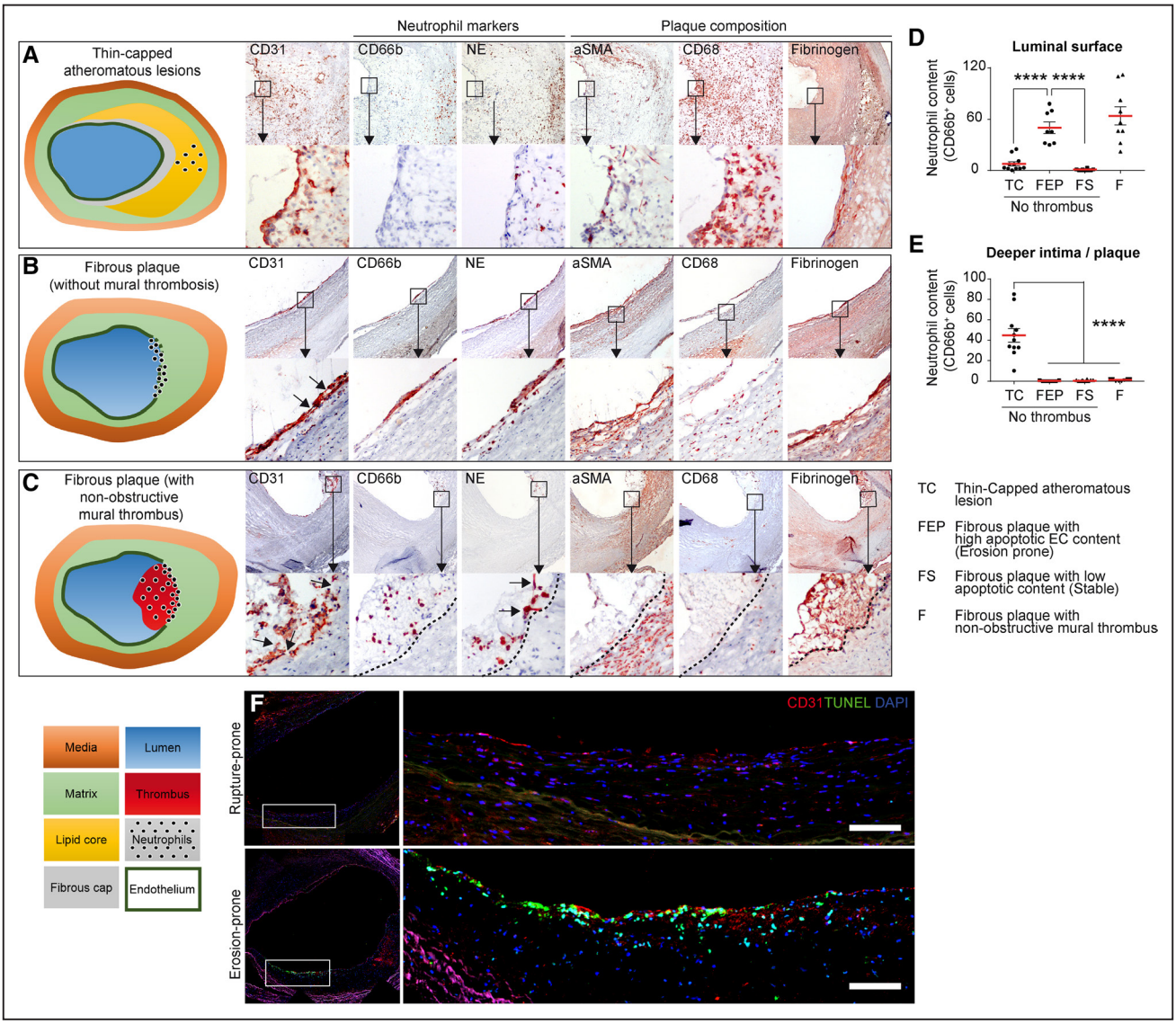

Figure 1. Neutrophils associate with the erosion-prone plaque morphology in humans. Human plaques with morphologies classified as thin-capped atheromatous lesions (n=11), fibrous without mural thrombosis (representing erosion-prone or healed or resorbing erosive thrombus; **B**), or fibrous plaques with nonobstructive mural thrombi (**C**), n=25, underwent serial cross-sectional analysis (×40 magnification) for endothelial cells (ECs)/platelets (CD31), neutrophils (CD66b) and neutrophil elastase (NE), and other cell types (smooth muscle cells, αSMA⁺) and macrophages (CD68⁺), and thrombus (fibrinogen). Insets show higher magnification (×100). CD66⁺ immunostaining quantified neutrophils located either on the luminal surface (**D**) or in the deeper intima/plaque (**E**). **F**, High content of apoptotic cells correlates with an erosion-prone morphology. Scale bars, 300 μm. Data are expressed as mean±SEM. ****P<0.0001. Mann–Whitney U test.

the fibrous plaques, regions of high neutrophil content colocalized with disruption of the EC monolayer (Figure 1B and 1C). In contrast, thin-capped atheromatous lesions generally had an intact endothelial lining and contained few if any neutrophils. Inspection of the deeper portions of plaques served as control for neutrophil content (Figure 1E). Further studies localized neutrophils in representative human atheromata with characteristics of superficial erosion. Double staining for myeloperoxidase (MPO) and CD61 showed neutrophils (MPO⁺) adjacent to but separate from platelets (CD61⁺). MPO/NE staining colocalized MPO with NE (Online Figure IB). Thus, neutrophil accumulation seems much more abundant in human lesions with erosion-prone characteristics than in those with features associated with fibrous cap rupture. Immunofluorescent staining showed a preferential accumulation of TUNEL⁺ cells in the intima, often colocalizing with CD31⁺ ECs, in erosion-prone plaques as compared with rupture-prone plaques (Figure 1F; Online Figure IC). Apoptotic ECs localized preferentially in the vicinity of NE⁺ neutrophils (Online Figure IC).

This study aimed to explore experimentally in vivo the mechanisms that underlie these findings in human plaques related to erosion versus rupture. To this end, we first tailored arteries to harbor matrix-rich fibrous intimas by injury followed by healing. We then subjected these arteries with preformed fibrous intimal lesions to flow perturbation induced by stenosis. The initial injury impaired EC permeability at day 0, and the EC layer recovered after a 4-week healing period (Figure 2A; Online Figure IIA), with local neointima formation (Figure 2A, right panel; Online Figure IIB). The intima/wall (media+adventitia) ratio increased significantly postinjury

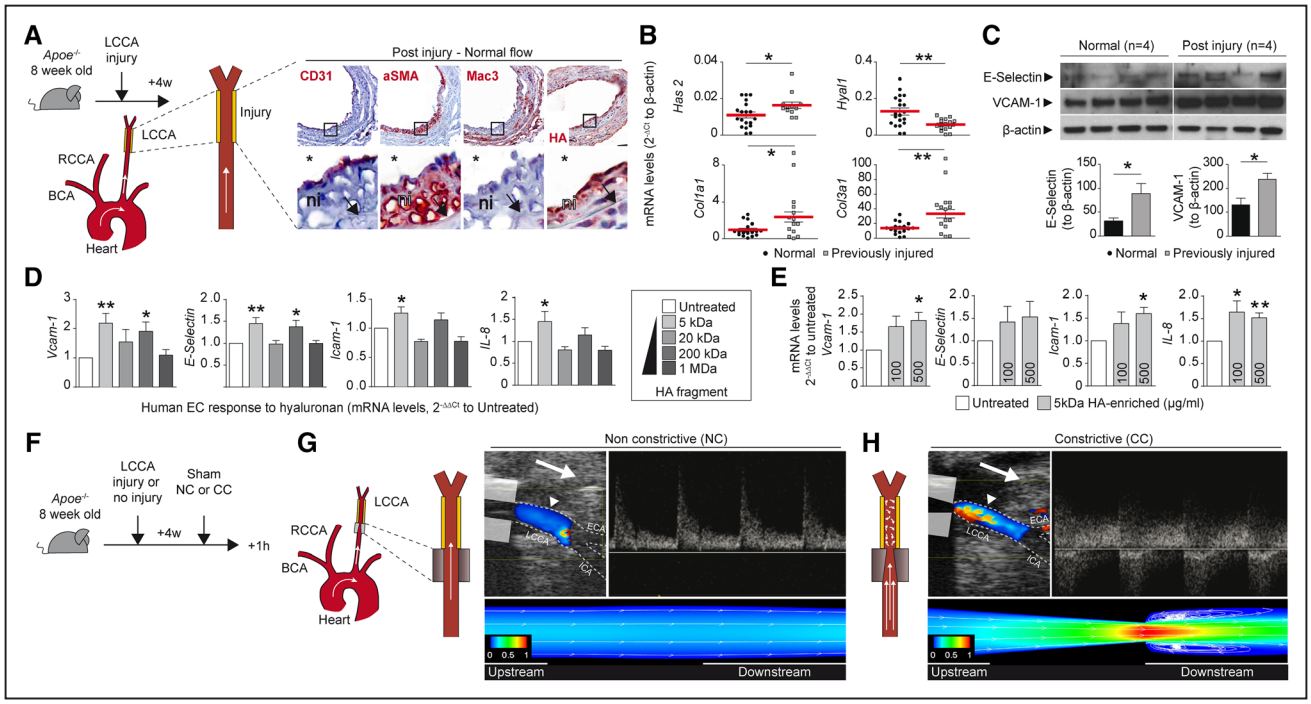

Figure 2. Creation of intimal lesions for experimental probing of mechanisms related to superficial erosion in mice. A, Experimental protocol showing carotid electric injury (yellow segment) performed at day 0 and followed in 4 weeks by endothelial reconstitution. Composition of the neointima in previously injured arteries in endothelial cells (ECs; CD31), vascular smooth muscle cells (SMA), macrophages (Mac3), and hyaluronan (HA). The insets show higher magnification views for each representative image. Carotid lumen (star) and internal elastic laminae (arrow) are shown. The arrow represents flow orientation. Quantitative polymerase chain reaction (QPCR) analysis was performed on normal vs previously injured carotid for the expression of extracellular matrix–related mRNAs (**B**). Data are expressed in $2^{-\Delta Ct}$ to β-actin. Each dot represents data from 1 animal. Mann–Whitney U test. **C**, Western blot and relative quantification showing overexpression of E-selectin and vascular cell adhesion molecule 1 (VCAM-1) in normal vs previously injured arteries, n=4. QPCR on lysates from human saphenous vein ECs cultured 48 h on native gelatin coating (untreated) vs coating enriched with hyaluronan (HA) of various molecular weights (**D**) or vs 100 or 500 μg/mL of 5 kDa HA-enriched coating (**E**). Data are expressed in $2^{-\Delta\Delta Ct}$ to untreated condition, mean±SEM, n=6 per group, $^{*}P<0.05$, $^{**}P<0.01$, $^{***}P<0.001$, and $^{****}P<0.0001$. Paired *t* test (**F**, **G**, and **H**). Placement of a cone-shape polyethylene cuff around the LCCA in mice and secured by a circumferential suture. Effect of nonconstrictive control cuff (**G**) or constrictive cuff placement on flow dynamics in carotid arteries (**H**). Doppler-coupled ultrasonography showing velocity patterns along the downstream flow (**left**, arrow) and the velocity peak downstream of the cuff (**right**, arrow) measured at 1.5 mm downstream of the cuff (arrowhead). Computational fluid dynamics using finite volume analysis verified the extent of flow perturbation and recirculation. Longitudinal cross-sectional simulation of the effect of a nonconstrictive cuff (**G**) or a constrictive cuff (**H**) showing a normalized axial velocity contour with superimposed velocity vectors (**G** and **H**). CC indicates constrictive cuff; ECA, external carotid artery; ICA, internal carotid artery; LCCA, left common carotid artery; NC, nonconstrictive cuff; ni, neointima; and RCCA, right common carotid artery.

compared with uninjured left common carotid arteries (LCCA; Online Figure IIB and IIC; $P<0.01$), but the media-to-wall ratio did not change significantly ($P=0.2$). Postinjury, LCCAs developed an SMC-rich neointima, with few macrophages, lacking a lipid core, and rich in HA (Figure 2A). This approach replicates key features of human plaques associated with superficial erosion[9] (Figure 1). Postinjury, arterial extracts contained significantly more mRNA encoding type I and type III collagen precursors and HA synthase 2 and decreased type I hyaluronidase mRNA, compatible with a slant toward HA accumulation (Figure 2B). E-selectin ($P<0.001$) and VCAM-1 ($P<0.0001$) expression remained elevated 4 weeks after injury, indicating persistent endothelial activation at these sites, as we previously observed in injured arteries in rabbits (Figure 2C; Online Figure IID).[33] Human saphenous vein ECs cultured on a gelatin substrate supplemented with various molecular weight fractions of HA showed increased EC responses to a 5 kDa fraction of HA (Figure 2D). Furthermore, human saphenous vein ECs cultured on a 5-kDa HA-enriched coating showed concentration-dependent activation (Figure 2E). Thus, regional electric injury induces SMC and HA-rich intimal hyperplasia, and exposure of the basal surface of EC to low molecular weight HA can chronically activate EC.

In Vivo Flow Perturbation

Placement of cone-shaped polyethylene cuffs around the adventitia of the LCCA modulated downstream flow (Figure 2F through 2H; Online Movie I). Placement of a nonconstrictive control cuff (NC) did not alter the flow velocity pattern (Figure 2G), but entailed the same operative manipulations and adventitial disturbance as the constrictive cuff (CC; Figure 2H). At peak systole (t=0.1 ms), computational flow dynamic analysis after NC placement showed a low variability in the velocity distribution of LCCA and unidirectional vectors along the length of the vessel (Figure 2G). In contrast, CC placement yielded a high variability in the velocity distribution downstream, producing multidirectional vectors (Online Figure IIG). The highest velocity occurred at the narrowest end of the cuff, and recirculation zones occurred

further downstream (Online Figure IIG). At peak systole, the LCCA with NC presented a low evenly distributed WSS profile (Online Figure IIH), whereas a high variability in the WSS distribution accompanied the CC placement, with increasing values observed along the cuff and lowest values immediately downstream (Online Figure II I). Time-averaged WSS plots obtained at sequential locations (Online Figure IIJ) showed no significant changes along the carotid in NC condition or proximal to the CC (site 1). Distal to the CC, mural WSS greatly increased at the narrowest cuff site (site 2), became negative with increased amplitude slightly downstream from cuff (site 3), and oscillated from positive to negative values further downstream from the cuff (site 4). These data show that flow restriction in carotid arteries produces oscillatory shear stress downstream, permitting controlled and characterized experimental manipulation of local hydrodynamics in normal arteries or those with tailored fibrous intimal hyperplasia.

Flow Perturbation Promotes Neutrophil Recruitment and Thrombus Formation in Previously Injured Arteries

Mice underwent placement of CC (n=45) or a NC (n=15) on either a normal or previously injured LCCA (Figure 3A and 3B; normal, n=19; post injury, n= 52). Control animals underwent a sham procedure (n=11). Neither NC placement nor sham procedure altered significantly intimal leukocyte accumulation downstream, demonstrating that neither the cuff material nor the surgical manipulations evoked acute inflammation. Neutrophils ($Ly6G^+$ cells) did, however, adhere to the arterial intima distal to the CC, much more in previously injured than in normal LCCA (Figure 3B; $P<0.001$). Further experiments extended the histological observations by flow cytometric analysis of luminal eluates of downstream arterial segments from previously injured arteries: segments of arteries experiencing flow perturbation had significantly increased $CD45^+Ly6G^+$ cells (CC; Figure 3C and 3D; $P<0.001$). $Ly6C^+$ monocytes also increased in the CC group, albeit 10-fold less than did neutrophils, illustrating the order-of-magnitude preponderance of neutrophils in this acute response (Figure 3C and 3D; $P<0.05$). $Ly6G^+$ cells lined sites of flow disturbance in LCCA (Figure 3E, downstream; Online Figure IVC and IVE). In contrast, upstream areas had few leukocytes. LCCA subjected to more prolonged flow perturbation (6 hour) still exhibited substantial $Ly6G^+$ cell accumulation, although the cell number declined 2-fold compared with that at 1 hour (Online Figure IV; P<0.001). Flow disturbance caused $Ly6G^+$ cell accumulation for up to 3 weeks (data not shown), compatible with chronic intimal disturbance. The adherent cells

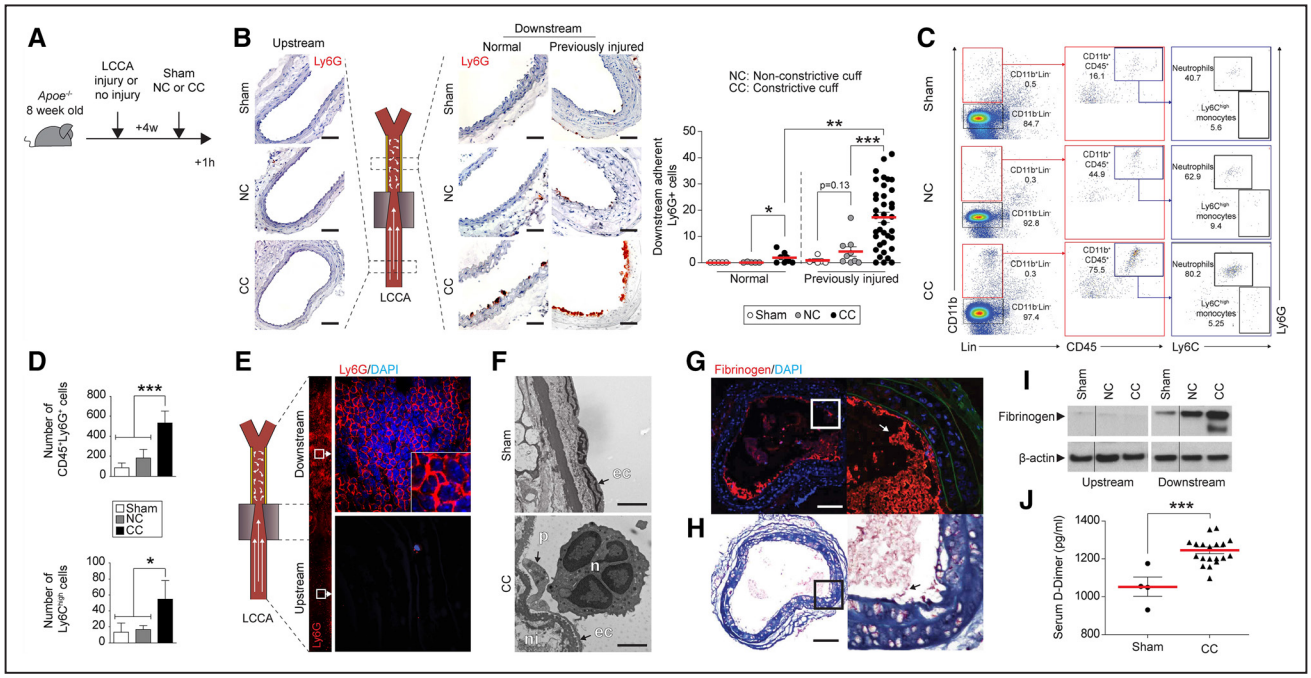

Figure 3. Flow perturbation promotes neutrophil recruitment and thrombus formation. A, Experimental protocol and time points studied. **B**, Ly6G immunohistochemical staining of LCCA downstream segments shows the accumulation of neutrophils 1 h after sham procedure (Sham; **upper**, n=9), placement of nonconstrictive cuff (NC; **intermediate**, n=14) or constrictive cuff (CC; **lower**, n=46) either on normal (**center**) or post-injured arteries (**right**). Uninjured upstream segments are shown on the **left**. The graph shows assessment of the number of adherent neutrophils to the intima. Scale bars: 30 μm. **C**, Flow cytometry performed on post-injured arteries after enzymatic digestion 1 h after sham procedure (**top**), placement of a NC (**middle**), or a CC (**bottom**). n=5 per group. Viable neutrophils were identified as $Lin^-CD45^+CD11b^+Ly6G^+$ and viable $Ly6C^{high}$ monocytes were identified as $CD45^+CD11b^+Ly6C^+$. **D**, Flow cytometric quantification of neutrophils and $Ly6C^{high}$ monocyte. $^*P<0.05$, $^{***}P<0.001$. **E**, Representative en face Ly6G immunofluorescent staining performed on previously injured LCCA subjected to flow perturbation (n=3). Segment downstream from the cuff (CC) is shown in higher magnification. **F**, Electron microscopic images show the intima of previously injured arteries after sham procedure (**top**) or CC placement (**bottom**). Scale bars, 2.5 nm. Immunofluorescent staining for fibrinogen (**G**) or Carstairs' staining (**H**) performed on a selection of postinjured LCCA that have formed intraluminal thrombus 1 h after flow perturbation. Scale bars, 100 μm. **I**, Immunoblotting showing elevated fibrinogen downstream of CC. Normalization, β-actin. **J**, Quantification by ELISA of circulating D-dimer concentrations in mice subjected to sham (n=4) vs flow perturbation (CC, n=19). Data are expressed as mean±SEM. Mann–Whitney U test. LCCA indicates left common carotid artery.

exhibited ultrastructural characteristics of neutrophils with segmented nuclei and plentiful cytoplasmic granules (Figure 3F). The CC groups displayed increased thrombus formation (Table II; P<0.05 and *P*<0.01) and fibrin-rich intraluminal thrombi in LCCAs after 1 hour of flow perturbation (Figure 3G and 3H). Arterial segments subjected to flow perturbation accumulated intimal fibrinogen (Figure 3I). Moreover, circulating D-dimer, a product of fibrin degradation, increased in the serum of mice from CC group after 1 hour of flow disturbance (Figure 3J). Finally, en face observation of the LCCA showed thrombus formation downstream of stenoses (Online Figure IVD). These results demonstrate that flow perturbation provokes local neutrophil and thrombus accumulation in arteries with fibrous intimal hyperplasia.

Flow-Mediated Neutrophil Recruitment Promotes Endothelial Injury

Sites of fatal superficial erosion complicating human atheromata show EC loss and neutrophil accumulation.[28] We, therefore, tested here the hypothesis that neutrophils contribute critically to loss of intimal EC in circumstances implicated in erosion. We examined the effect of 6 hours of continuous flow perturbation on luminal endothelium in arteries with fibrous thickened intimas (Figure 4A). In comparison to controls, in the CC group, VCAM-1 and E-selectin protein increased in extracts of downstream arterial segments (Figure 4B). Flow perturbation also promoted disturbed EC barrier function (Figure 4C; *P*<0.01) and apoptosis (Figure 4D). Further immunostaining using an anticleaved-caspase-3 antibody buttressed these findings (Online Figure IXB). Locally, ECs showed ultrastructural features of dying cells, including blebbing and vacuolization (Figure 4E). Flow perturbation significantly decreased endothelial continuity (*P*<0.05), altered EC morphology, and led to EC desquamation (Figure 4F and 4H; *P*<0.05). Discontinuity in the intimal endothelium correlated with the number of firmly adherent neutrophils (Figure 4G). Numerous neutrophils also congregated with activated EC or colocalized with patches of intimal denudation (Figure 4I).

Further experiments assessed the causal relationship between neutrophil presence and endothelial dysfunction/loss (Figure 4J). Anti-Ly6G blocking antibody treatment 24 hours before cuffing induced neutropenia (N=11). Alternatively, administration of an anti-LFA-1 (lymphocyte function-associated antigen 1) blocking antibody 1 hour before the experiment aimed to reduce neutrophil recruitment. Either treatment abolished the recruitment of $Ly6G^+$ neutrophils in the LCCA after 1 or 6 hours of flow perturbation (Figure 4K). After 6 hours of flow perturbation, either antineutrophil treatment likewise limited endothelial permeability in the arterial segments subjected to disturbed flow (Figure 4L), decreased the number of luminal $CD31^+TUNEL^+$ apoptotic EC (Figure 4M; *P*<0.05), and preserved endothelial continuity (Figure 4N; *P*<0.05). These results identify neutrophils as effectors of EC injury, death, and detachment under circumstances associated with thrombosis because of superficial erosion.

Endogenous TLR2 Activates EC and Promotes Neutrophil Chemoattraction

Further experiments tested the hypothesis that TLR2 participates in EC activation and potentiates neutrophil chemoattraction or leukocyte adhesion in arteries that share features of eroded human atheromata. Human saphenous vein ECs incubated with the TLR2 agonist Pam3CSK4 (Pam3) or with vehicle showed time-dependent increases in VCAM-1, ICAM-1 (intercellular adhesion molecule 1), E-selectin, and interleukin-8 (Figure 5A). Six hours after Pam3 or vehicle administration intraperitoneally to apolipoprotein E-deficient ($Apoe^{-/-}$) or $Apoe^{-/-}Tlr2^{-/-}$ mice, luminal eluates, and extracts of the remaining aorta wall (intima excluded) underwent RNA isolation and quantitative polymerase chain reaction analysis (Figure 5B). Arterial luminal eluates from Pam3-treated $Apoe^{-/-}$ mice showed significantly increased *Vcam-1*, *E-selectin*, chemokine (C-X-C motif) ligand (*Cxcl-1*), *Cxcl-2*, and *Cxcl-5* mRNAs (Figure 5C). Aortic tunica media extracts from Pam3-treated $Apoe^{-/-}$ mice had increased concentrations of the chemoattractants *Cxcl-1*, *Cxcl-2*, and *Cxcl-5* mRNAs but not messages that encode the endothelial adhesion molecules *Vcam-1* or *E-selectin*. Pam3 did not exert these actions in $Apoe^{-/-}Tlr2^{-/-}$ animals, indicating that these arterial responses to Pam3 depend on TLR2. The *Bax/Bcl2* mRNA ratio also increased in these intimal extracts, implicating TLR2 in endothelial apoptosis in vivo (Figure 5D). Pam3 administration augmented both VCAM-1 and E-selectin protein in aortas isolated from $Apoe^{-/-}$ mice, but not in $Apoe^{-/-}Tlr2^{-/-}$ animals (Figure 5E), and selectively activated luminal EC in vivo (Figure 5F). Circulating CXCL-1 also increased in Pam3-treated $Apoe^{-/-}$ but not in $Apoe^{-/-}Tlr2^{-/-}$ animals (Figure 5G). Together, these results indicate that TLR2 activation leads to the overexpression of neutrophil chemoattractants by both EC and mesenchymal cells, while it increases EC expression of leukocyte adhesion molecules and augments luminal EC apoptosis.

Testing the hypothesis that TLR2 of arterial origin participates in the recruitment of neutrophils used chimeric mice constructed by transplantation of either $Apoe^{-/-}$ or $Apoe^{-/-}Tlr2^{-/-}$ bone marrow to lethally irradiated $Apoe^{-/-}$ or $Apoe^{-/-}Tlr2^{-/-}$ recipients. Mice from each of the 4 groups, thus, generated (Figure 5H) received Pam3 or vehicle and underwent analysis after 6 hours (Figure 5I). Eluates from aortic luminal extracts furnished RNA for quantitative polymerase chain reaction analysis (Figure 5I). As expected, Pam3 injection strongly activated luminal cells in mice expressing TLR2 in both intrinsic arterial and bone marrow–derived cells (group 1; Figure 5J) but not in $Tlr2^{-/-}$ mice (group 4). Animals lacking TLR2 in bone marrow–derived cells alone (group 3) retained responsiveness to Pam3, to an extent comparable with mice from group 1. In contrast, mice lacking TLR2 in intrinsic arterial cells, but reconstituted with bone marrow from TLR2-sufficient animals (group 2), showed a much lower activation than group 1 mice. While Pam3 increased circulating CXCL-1 in groups 1, 2, and 3, group 2 showed significantly lower blood concentration of CXCL-1 compared with groups 1 and 3 (Figure 5K; *P*<0.001). Pretreatment with Pam3 strongly increased TLR2 expression in luminal ECs (Online Figure VIII). Immunofluorescent colocalization by confocal microscopy reveals that ECs express most arterial TLR2, although adherent neutrophils and some SMCs also show limited positivity. A 3-dimensional

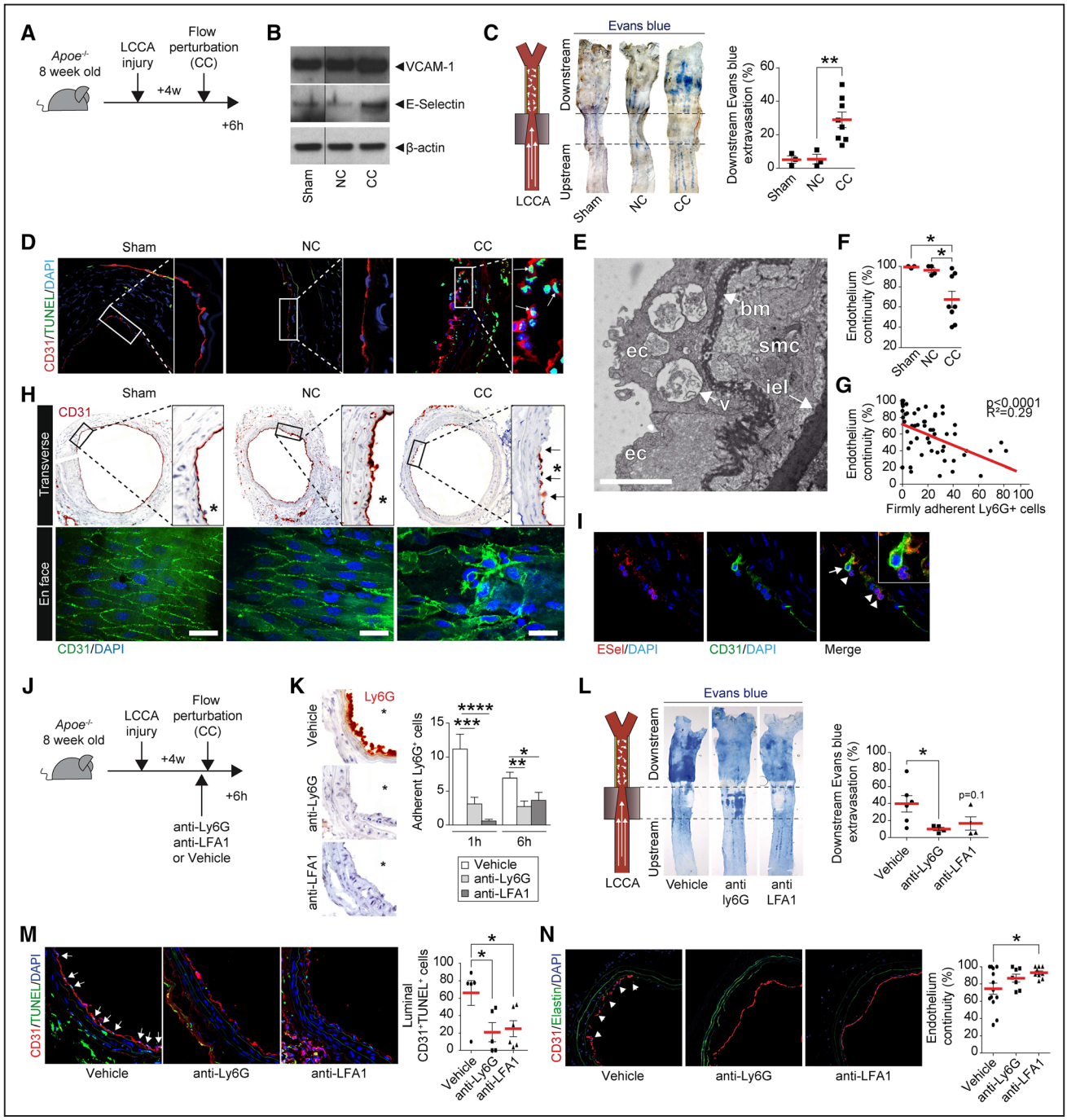

Figure 4. Flow-mediated neutrophil recruitment potentiates endothelial cell dysfunction and loss. A, Experimental protocol and time points studied: left common carotid artery (LCCA) were subjected to injury and 4 weeks later to 6 h of flow perturbation (constrictive cuff [CC]). Sham, nonconstrictive cuff (NC), or CC arteries probed for the expression of vascular cell adhesion molecule 1 (VCAM-1) and E-selectin by Western blot (**B**) or for Evans blue extravasation (**C**). Normalization, β-actin. **D**, Immunofluorescent staining for endothelium (CD31), apoptosis (TUNEL), and DNA (DAPI) in cross sections of Sham, NC, or CC arteries. Each image shows higher magnification on the right. Arrows show the presence of luminal apoptotic endothelial cells (ECs). **E**, Electron microscopy image showing ECs subjected to flow perturbation in previously injured arteries. Scale bars, 2 μm. **F**, Quantification of endothelial continuity. **G**, Negative correlation between endothelial continuity and the number of adherent Ly6G⁺ neutrophils (P<0.0001, R^2=0.29). Immunohistochemical staining for CD31 (**top**) or en face visualization in immunofluorescence of EC (CD31) and DNA (DAPI; **bottom**) in downstream arteries after sham procedure (**left**, n=3), placement of a nonconstrictive cuff (**middle**, n=4), or constrictive cuff (**right**, n= 8). Scale bars, 20 μm. Arrows show patches of EC denudation. Semiquantitative assessment of endothelial continuity cross sections CD31 immunohistochemistry is shown in the graph (**right**). **I**, Immunofluorescent stainings for E-selectin, EC (CD31), and DNA (DAPI) show EC undergoing detachment (arrow), in contact with neutrophils (arrowhead) in arteries subjected to flow perturbation (CC). **J**, Experimental protocol and time points showing LCCA subjected to injury, followed 4 weeks later by systemic injections of neutralizing Ly6G antibody, LFA-1 (lymphocyte function-associated antigen 1) antibody, or vehicle before flow perturbation (CC). **K**, Ly6G staining in immunohistochemistry shows neutrophil recruitment after 1 h of flow perturbation in LCCA subjected to flow in groups receiving vehicle, anti-Ly6G, or anti-LFA-1. The graph shows quantification of adherent neutrophils in each group, after either 1 or 6 h of flow perturbation. **L**, LCCA from group vehicle, anti-Ly6G, and anti-LFA-1 probed for (*Continued*)

Figure 4 Continued. endothelial permeability using Evans blue intravital staining after 6 h of flow perturbation. **M**, Immunofluorescent staining for endothelium (CD31, red), early apoptosis (green), and DNA (DAPI, blue) shows luminal endothelial apoptotic cells (arrows) in group vehicle, anti-Ly6G, or anti-LFA-1 after 6 h of flow perturbation. **N**, Immunofluorescent staining for endothelium (CD31, red), elastin autofluorescence (green), and DNA (DAPI, blue) shows endothelial continuity in group vehicle, anti-Ly6G, or anti-LFA-1 after 6 h of flow perturbation. Data are expressed as mean±SEM. **P*<0.05, ***P*<0.01, ****P*<0.001, and *****P*<0.0001. Mann–Whitney U test. bm indicates basement membrane; ec, endothelial cell; iel, internal elastic laminae; smc, smooth muscle cell; and v, vacuole.

reconstruction revealed that TLR2 localizes mainly on the basal surface of ECs in contact with the basement membrane (Online Movie I). In contrast, the apical surface of EC did not contain TLR2. These results demonstrate that TLR2 expressed by intrinsic arterial cells participates prominently in intimal cell activation and supports the hypothesis that endothelial TLR2 promotes neutrophil recruitment in the context of superficial erosion.

TLR2 Participates in Neutrophil Recruitment, EC Death, and Dysfunction in Arteries With Fibrous Intimal Hyperplasia in Response to Flow Disturbance

Areas of disturbed arterial flow in mouse and human atheromata exhibit overexpression of TLR2. These observations and the ability of TLR2 ligation to activate ECs suggested the hypothesis that TLR2 participates in the recruitment of intimal

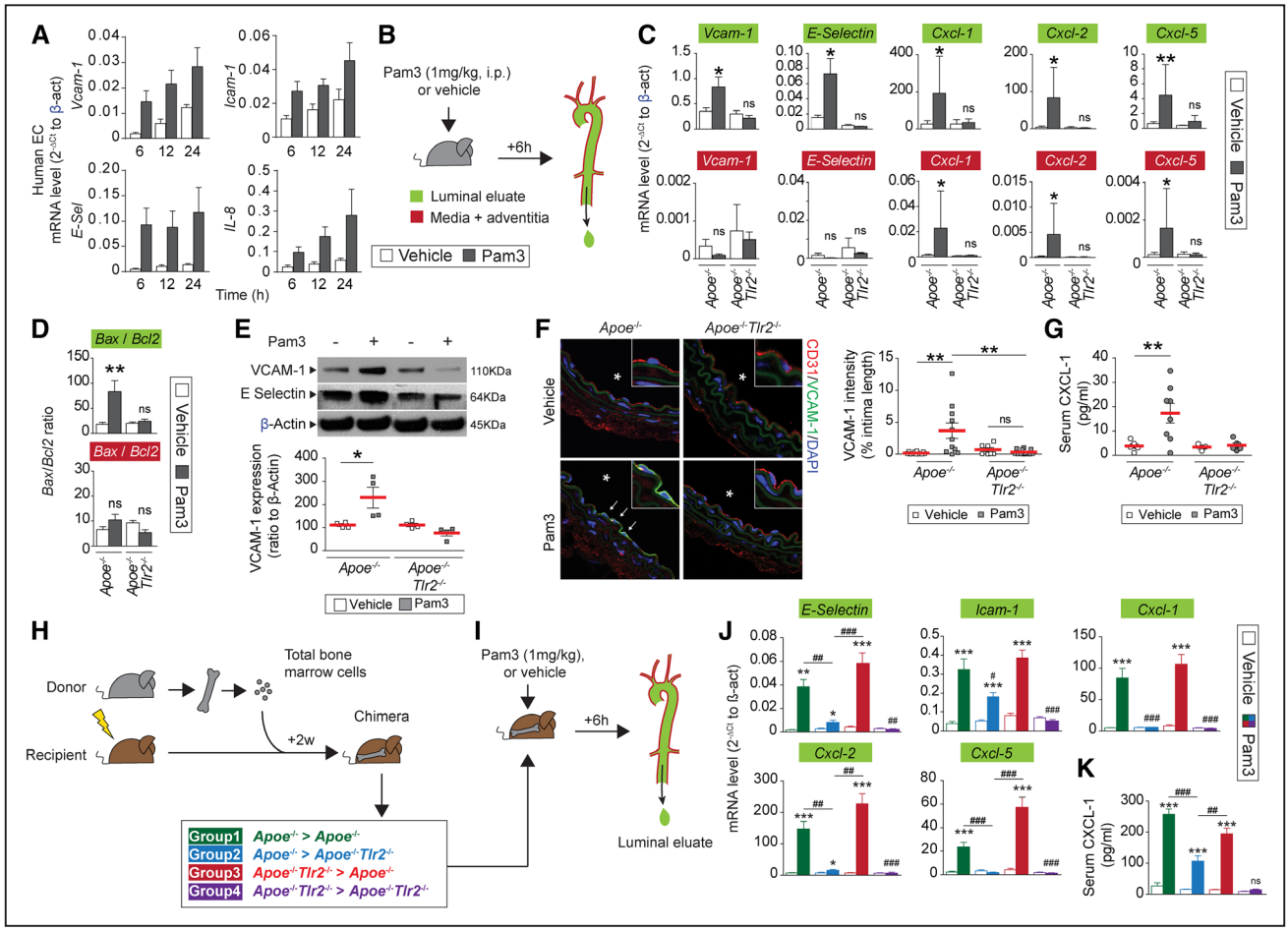

Figure 5. TLR2 mediates endothelial cell activation in vivo. A, Quantitative polymerase chain reaction (PCR) on lysates from human saphenous vein endothelial cells (ECs) 6, 12 or 24 h after Pam3csk4 incubation, n=6 per condition. **B**, Experimental protocol and time points used in the study. **C** and **D**, Quantitative PCR performed on aortic luminal eluates (**top**, green) or media-adventitia lysates (**bottom**, red) isolated 6 h after Pam3csk4 (Pam3, gray bars) or vehicle (white bars) injection in either *Apoe*$^{-/-}$ or *Apoe*$^{-/-}$*Tlr2*$^{-/-}$ mice, n=6 per condition. **C**, mRNA expression of adhesion molecules and neutrophil chemoattractants. **D**, mRNA expression ratio between *Bax* and *BCl2*. **E**, Immunoblotting for vascular cell adhesion molecule 1 (VCAM-1), E-selectin performed on aorta after Pam3 (gray bars) or vehicle (white bars) injection in either *Apoe*$^{-/-}$ or *Apoe*$^{-/-}$*Tlr2*$^{-/-}$ mice. Normalization used β-actin. The graph shows quantification of VCAM-1 expression (**below**). **F**, Immunofluorescent staining for endothelium (CD31), VCAM-1, and DNA (DAPI) in LCCA isolated from *Apoe*$^{-/-}$ (**left**) or *Apoe*$^{-/-}$*Tlr2*$^{-/-}$ mice (**right**) 6 h after injection of vehicle (**top**) or Pam3 (**bottom**). The stars indicate the lumen and the arrows show EC overexpressing VCAM-1. The graph (**right**) depicts semiquantitatively VCAM-1 immunopositivity in luminal EC expressed as percent of intima length. **G**, Quantification by ELISA of circulating chemokine (C-X-C motif) ligand (CXCL-1) levels. **H**, Generation of 4 groups of chimeric mice and experimental protocol of the study (**I**). Quantitative PCR performed on luminal eluate (**J**) and quantification by ELISA of CXCL-1 serum levels (**K**) isolated from mice from each group, 6 h after vehicle (white bars) or Pam3 injection (colored bars), n=5 to 6 per condition. Data are expressed as mean±SEM. **P*<0.05, ***P*<0.01, ****P*<0.001, and *****P*<0.0001, Pam3 vs vehicle. ##*P*<0.01, ###*P*<0.001, comparison of selected groups, paired *t* test. ApoE indicates apolipoprotein E; CXCL, chemokine (C-X-C motif) ligand; IL, interleukin; and TLR2, Toll-like receptor 2.

neutrophils. Eight-week-old *Apoe*$^{-/-}$ or *Apoe*$^{-/-}$*Tlr2*$^{-/-}$ mice first underwent LCCA injury (Figure 6A). LCCA with fibrous intimal thickening in *Apoe*$^{-/-}$ versus *Apoe*$^{-/-}$*Tlr2*$^{-/-}$ showed no significant differences in internal or external diameter or in the intima-to-wall ratio (P=0.2; Figure 6B and 6C). *Tlr2* deficiency in normal or previously injured arteries did not affect the

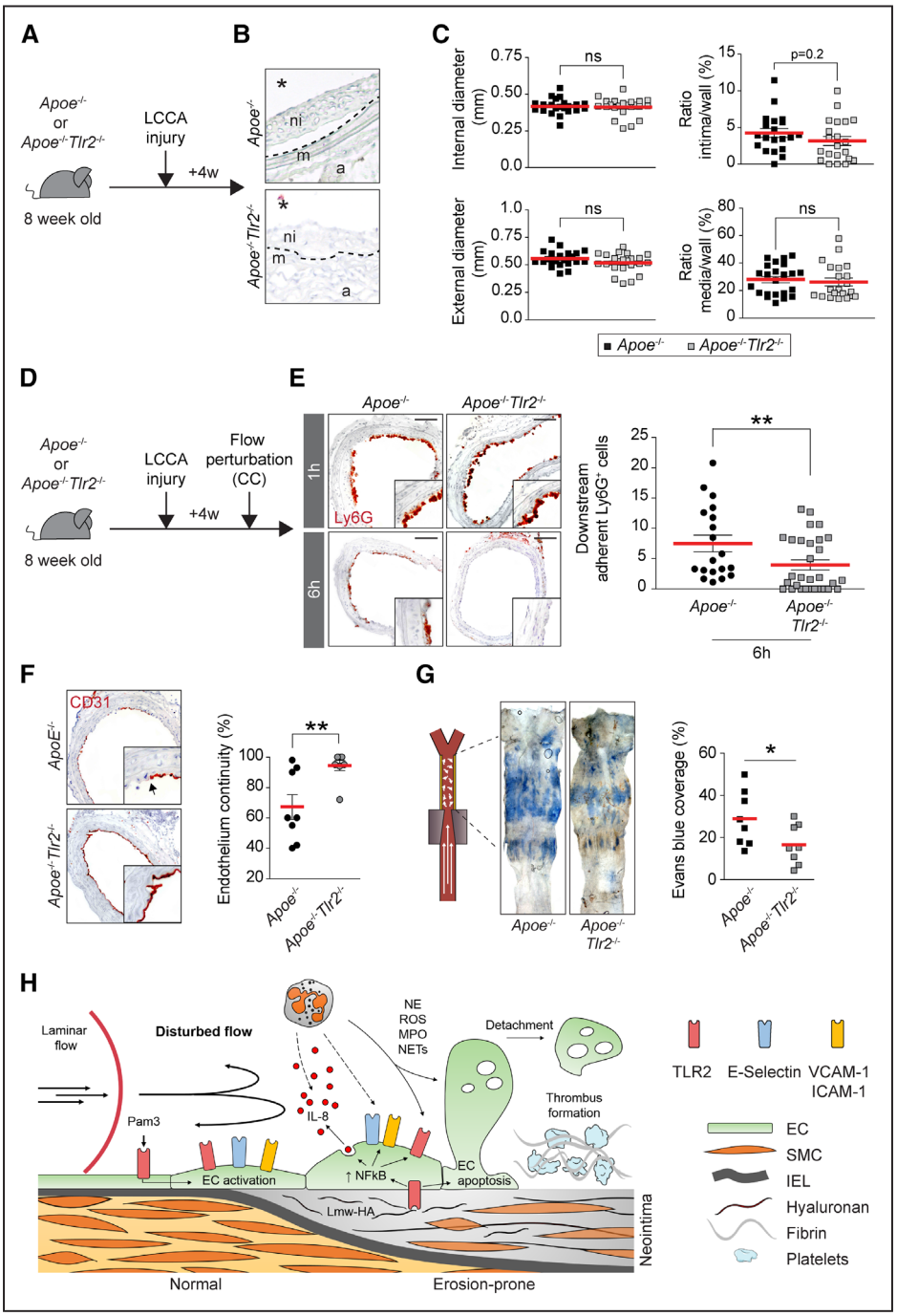

Figure 6. Flow perturbation promotes neutrophil recruitment through TLR2. **A**, Experimental timeline. **B**, Hematoxilin and eosin (H&E) staining shows neointima formation after left common carotid artery (LCCA) injury in *Apoe*$^{-/-}$ and *Apoe*$^{-/-}$*Tlr2*$^{-/-}$ mice. The star indicates the lumen. **C**, Morphometric analysis showing measurement of internal (**top, left**) and external diameters (**bottom, left**) and the ratio intima/wall (**top, right**) and media/wall (**bottom, right**). **D**, Experimental protocol involving LCCA injury followed by flow perturbation (CC) in *Apoe*$^{-/-}$ and *Apoe*$^{-/-}$*Tlr2*$^{-/-}$ mice. **E**, Ly6G immunohistochemistry staining of LCCA cross-sections showing the recruitment of neutrophils 1 or 6 h after flow perturbation in *Apoe*$^{-/-}$ and *Apoe*$^{-/-}$*Tlr2*$^{-/-}$ mice. The graph shows the semiquantitative assessment of adherent neutrophils to the intima after 6 h of flow perturbation. Scale bar: 60 μm. **F**, CD31 immunohistochemistry staining shows endothelium. The graph (**right**) shows assessment of endothelial continuity. **G**, LCCA isolated from *Apoe*$^{-/-}$ and *Apoe*$^{-/-}$*Tlr2*$^{-/-}$ mice were probed for endothelial permeability using Evans blue intravital staining after 6 h of flow perturbation. **H**, Summary diagram of the main findings of this study. Data are expressed as mean±SEM. *P<0.05, **P<0.01. Mann–Whitney U test. a indicates adventitia; CC, constrictive cuff; IEL, internal elastic lamina; Lmw-HA, low molecular weight–hyaluronan; m, media; MPO, myeloperoxidase; ni, neointima; NE, neutrophil elastase; NETs, neutrophil extracellular traps; NF-κB, nuclear factor-κB; ROS, reactive oxygen species; SMC, smooth muscle cell; and TLR2, Toll-like receptor 2.

arterial expression of the atherothrombosis-related genes evaluated (Online Figure VC). Other mice underwent LCCA injury followed 4 weeks later by flow perturbation (Online Figure VID). While local neutrophil number did not differ between groups after 1 hour (Online Figure VD), after 6 hours, the distal arterial segments of *Apoe*$^{-/-}$*Tlr2*$^{-/-}$ contained significantly fewer Ly6G^{+} neutrophils than *Apoe*$^{-/-}$ (Figure 6E; $P<0.01$). Furthermore, *Apoe*$^{-/-}$*Tlr2*$^{-/-}$ mice showed less disruption in endothelial continuity in arterial segments subjected to flow perturbation (Figure 6F), as well as decreased permeability (Figure 6G). *Apoe*$^{-/-}$*Tlr2*$^{-/-}$ mice had reduced local thrombus formation after 1 or 6 hours of flow perturbation (Online Table II) and diminished circulating D-dimer concentrations after 6 hours of flow perturbation (Online Figure IIIE). These results support the participation of TLR2 in the recruitment of neutrophils, in EC dysfunction/loss, and in subsequent thrombosis in the context of superficial erosion (Figure 6H).

Discussion

Superficial erosion causes arterial thrombosis, and hence ACS, without plaque rupture, as disclosed by postmortem examination and optical coherence tomographic imaging in intact patients. Studies of human autopsy specimens do not permit dissection of the mechanisms that underlie this modus of thrombotic complication of atherosclerosis. This study extends in vivo our prior in vitro observations that implicated TLR2 signaling, engagement of this innate immune receptor by HA or other ligands, and the participation of neutrophils in aspects of superficial erosion.

Among several processes that may contribute to superficial erosion, flow perturbation can promote endothelial dysfunction and death. Yet, areas subjected solely to flow perturbation seldom develop superficial erosion, suggesting that flow disturbance alone does not suffice to trigger thrombosis. We, therefore, recently proposed a 2-hit schema for the pathogenesis of superficial erosion, a mechanism of coronary thrombosis apparently on the rise.[5,28] Plaques that have precipitated thrombi because of erosion differ distinctly from the so-called rupture-prone plaque. These differences suggest striking divergences in the pathological mechanisms and support the concept that plaque composition influences the mode of thrombotic complication. This in vivo study used an experimental approach designed to mimic certain characteristics of plaques that have caused thrombosis because of superficial erosion. We created in mouse arteries expanded intimas enriched in SMC and a glycosaminoglycan-rich extracellular matrix with few inflammatory cells, which recapitulates some key features of the substrate associated with eroded plaques in humans.[8,9] We used ApoE-deficient mice consuming a chow rather than atherogenic diet to avoid producing plaques overloaded with lipids and macrophage foam cells, characteristics of ruptured rather than eroded lesions.[34] The use of electric injury to stimulate intimal expansion proved more reproducible in extensive pilot experiments than did endovascular intervention. The resultant lesions accumulated HA and exhibited altered HA turnover, as indicated by reciprocal changes in the concentrations of mRNAs that encode enzymes involved in HA production and degradation. Heightened expression of E-selectin and VCAM-1 in these arteries indicated sustained chronic EC activation, findings concordant with our prior work on injured rabbit arteries.[33] Other studies have shown HA accumulation during neointimal hyperplasia in association with the migration and the proliferation of SMC and that intimal HA may accentuate atherosclerosis.[35,36] In vitro, a culture substrate enriched with low molecular weight HA caused low-level activation of human ECs, consistent with the notion that intimal HA could pave the way for thrombotic complication because of superficial erosion. Prior in vitro studies have seldom aimed to replicate the hydrodynamic conditions that prevail downstream of arterial stenosis in humans. The current in vivo findings show that flow disturbance sets the stage for thrombosis in arteries with fibrous intimal thickening.

Disturbed flow and low shear stress can activate arterial ECs through nuclear factor-κB[37,38] and also rapidly augment P-selectin and interleukin-8 elaboration nontranscriptionally by triggering their translocation to the EC luminal surface.[39] Experimental stenosis in veins promotes the accumulation of neutrophils that participate in P-selectin-dependent initiation/amplification of thrombosis.[40] Here, arterial ECs exposed to flow perturbation displayed markers of activation and apoptosis acutely and developed patches of endothelial desquamation. Oscillatory shear stress can induce EC apoptosis through various pathways, including p53 and protein kinase C-ζ.[18,41] Apoptosis could in turn exacerbate EC detachment and promote thrombosis.

Substantial neutrophil accumulation distal to stenosis occurred in the arteries with fibrous intimal expansion. Interruption of neutrophil trafficking protected EC from activation, apoptosis, and detachment. These observations support the local recruitment of neutrophils in eroded plaques and their role in extending injury,[28,42] whether or not these leukocytes participate in plaque formation.[43] Neutrophil arrival at sites of early erosion could, thus, amplify and propagate conditions that promote local thrombosis, in accord with our proposed 2-hit scheme. Granulocytes can harm EC in many ways,[44] including by producing proteinases that sever the tethers of the ECs to the basement membrane favoring desquamation.[45] Neutrophils strongly activate cultured ECs, disturb their ability to adhere to the basement membrane, and disturb EC morphology.[28,44] NE can degrade basement membrane constituents,[46] enhance EC injury,[47] and favor anoikis and apoptosis,[48] and concentrations of this enzyme increase in patients with myocardial infarction.[49] Neutrophils also contain abundant MPO, an enzyme that produces hypochlorous acid, an inducer of EC apoptosis and tissue factor production.[30] While a subset of recruited cells after flow perturbation express MPO in this study, MPO does not necessarily colocalize with Ly6G^{+} neutrophils. Rather, in mice, macrophages contain considerable MPO, an example of the discrepancy between murine and human innate immunity.

Dying granulocytes also generate NETs, structures that can induce EC death and dysfunction.[50,51] NETs could also promote EC detachment as they contain matrix metalloproteinase-9, a metalloproteinase involved in the degradation of the basement membrane type IV collagen and are able to activate endothelial pro-matrix metalloproteinase-2.[51] We previously reported the presence of NETs and NE at the surface of human plaques resembling those implicated in superficial

erosion.[28] NETs contain tissue factor procoagulant and can further furnish scaffolds for coronary thrombi in culprit lesions of ACS.[52,53]

This study demonstrates in vivo that TLR2 participates in EC activation and amplifies the recruitment of neutrophils after flow perturbation. ECs express TLR2 that participates in experimental atherosclerosis. TLR2 also localizes in human atheromata with characteristics of those that have caused thrombosis because of erosion.[28] Previous studies showed that low molecular weight fractions of HA can activate TLR2 signaling through a nuclear factor-κB–dependent pathway.[27] Thus, HA could act as an endogenous agonist of TLR2 and contribute to neutrophil recruitment in the setting of disturbed flow, as supported by the present findings. The use of chimeric mice indicates that TLR2 expressed by intrinsic arterial cells rather than leukocytes mediates the release of neutrophil chemoattractants and the production of endothelial adhesion molecules. In addition to TLR2, HA can also bind various receptors, including CD44 or ICAM-1. Flow perturbation could also activate alternative signaling (ie, by integrins) that may synergize with constitutive TLR2 signaling driven by HA binding. Defining the roles of these and other potential pathways will require further study.

The lack of experimental tools in vivo for studying superficial erosion has constituted a considerable hindrance and contributes to the knowledge gap in the field. The experimental approach used here permitted us to test hypotheses in vivo regarding the pathogenesis of superficial erosion that emerged from in vitro or descriptive observations made by our laboratory and others. This in vivo approach permitted testing of focused mechanistic hypotheses related to the pathophysiology of superficial erosion. The short time course of the experiments presented here represents one of several limitations to the ready extrapolation of our results to a human disease that plays out over decades. Yet, these findings furnish some early and novel insights into the mechanisms of superficial erosion, a major gap area in our understanding of the thrombotic complications of human atherosclerosis. This quest has become increasingly clinically compelling because current therapies have made substantial inroads in reducing plaque rupture and because superficial erosion has emerged as a considerable continuing contributor to residual risk in the current era.[5,54,55]

Acknowledgments

We thank David Lynn, Marc Belanger, Mark MacMillan, and Chelsea Swallom for providing administrative, technical, and editorial support throughout the project. G. Franck, K.J. Croce, and P. Libby designed the research studies; G. Franck, T. Mawson, G. Sausen, G.S. Masson, Y. Tesmenitsky, and E. Shvartz conducted the experiments; G. Franck, T. Mawson, G. Sausen, M. Salinas, G.S. Masson, A. Cole, M. Beltrami-Moreira, and T. Quillard acquired the data; G. Franck, G. Sausen, M. Salinas, G.S. Masson, and M. Nahrendorf analyzed the data; M. Salinas, Y. Chatzizisis, G. Sausen, F.K. Swirski, M. Nahrendorf, E. Aikawa, K.J. Croce, and P. Libby advised regarding the experimental design; and G. Franck and P. Libby wrote the article.

Sources of Funding

This work was supported by grants from the National Heart, Lung and Blood institute (NIH-R01 HL080472) by the Leducq Foundation (Paris, France) and from the RRM charitable fund. G. Franck was supported by the Harold M. English Fellowship Fund from Harvard Medical School (Boston, USA), the Fondation Bettencourt Schueller (Neuilly-sur-Seine, France), and the Philippe Foundation (New York, USA, and Paris, France). T. Mawson received support from the Sarnoff Cardiovascular Research Foundation (Great Falls, USA). G. Sausen received financial support from the Coordenação de Aperfeiçoamento de Pessoal de Nível Superior and the Lemann Foundation (Brazil). M. Beltrami-Moreira received support from the Lemann Foundation and the National Council for Scientific and Technological Development (CNPq, Brazil). E. Aikawa was supported by grants from the National Heart, Lung and Blood Institute (NIH-R01 HL114805 and NIH-R01 HL109506). We thank Pr Ronglih Liao and Dr Sudeshna Fisch from the Brigham and Women's Hospital Cardiovascular Physiology Core for assistance in ultrasound visualization.

Disclosures

None.

References

1. Libby P. Mechanisms of acute coronary syndromes. *N Engl J Med*. 2013;369:883–884. doi: 10.1056/NEJMc1307806.
2. Bentzon JF, Otsuka F, Virmani R, Falk E. Mechanisms of plaque formation and rupture. *Circ Res*. 2014;114:1852–1866. doi: 10.1161/CIRCRESAHA.114.302721.
3. Libby P. How does lipid lowering prevent coronary events? New insights from human imaging trials. *Eur Heart J*. 2015;36:472–474. doi: 10.1093/eurheartj/ehu510.
4. van Lammeren GW, den Ruijter HM, Vrijenhoek JE, van der Laan SW, Velema E, de Vries JP, de Kleijn DP, Vink A, de Borst GJ, Moll FL, Bots ML, Pasterkamp G. Time-dependent changes in atherosclerotic plaque composition in patients undergoing carotid surgery. *Circulation*. 2014;129:2269–2276. doi: 10.1161/CIRCULATIONAHA.113.007603.
5. Libby P, Pasterkamp G. Requiem for the 'vulnerable plaque'. *Eur Heart J*. 2015;36:2984–2987. doi: 10.1093/eurheartj/ehv349.
6. Jernberg T, Hasvold P, Henriksson M, Hjelm H, Thuresson M, Janzon M. Cardiovascular risk in post-myocardial infarction patients: nationwide real world data demonstrate the importance of a long-term perspective. *Eur Heart J*. 2015;36:1163–1170. doi: 10.1093/eurheartj/ehu505.
7. Jia H, Abtahian F, Aguirre AD, et al. In vivo diagnosis of plaque erosion and calcified nodule in patients with acute coronary syndrome by intravascular optical coherence tomography. *J Am Coll Cardiol*. 2013;62:1748–1758. doi: 10.1016/j.jacc.2013.05.071.
8. Virmani R, Kolodgie FD, Burke AP, Farb A, Schwartz SM. Lessons from sudden coronary death: a comprehensive morphological classification scheme for atherosclerotic lesions. *Arterioscler Thromb Vasc Biol*. 2000;20:1262–1275.
9. Falk E, Nakano M, Bentzon JF, Finn AV, Virmani R. Update on acute coronary syndromes: the pathologists' view. *Eur Heart J*. 2013;34:719–728. doi: 10.1093/eurheartj/ehs411.
10. Kolodgie FD, Burke AP, Farb A, Weber DK, Kutys R, Wight TN, Virmani R. Differential accumulation of proteoglycans and hyaluronan in culprit lesions: insights into plaque erosion. *Arterioscler Thromb Vasc Biol*. 2002;22:1642–1648.
11. Chien S, Li S, Shyy YJ. Effects of mechanical forces on signal transduction and gene expression in endothelial cells. *Hypertension*. 1998;31:162–169.
12. Chatzizisis YS, Coskun AU, Jonas M, Edelman ER, Feldman CL, Stone PH. Role of endothelial shear stress in the natural history of coronary atherosclerosis and vascular remodeling: molecular, cellular, and vascular behavior. *J Am Coll Cardiol*. 2007;49:2379–2393. doi: 10.1016/j.jacc.2007.02.059.
13. Gimbrone MA Jr, García-Cardeña G. Endothelial cell dysfunction and the pathobiology of atherosclerosis. *Circ Res*. 2016;118:620–636. doi: 10.1161/CIRCRESAHA.115.306301.
14. Fry DL. Acute vascular endothelial changes associated with increased blood velocity gradients. *Circ Res*. 1968;22:165–197.
15. Joris I, Zand T, Majno G. Hydrodynamic injury of the endothelium in acute aortic stenosis. *Am J Pathol*. 1982;106:394–408.
16. Tricot O, Mallat Z, Heymes C, Belmin J, Lesèche G, Tedgui A. Relation between endothelial cell apoptosis and blood flow direction in human atherosclerotic plaques. *Circulation*. 2000;101:2450–2453.
17. Chaudhury H, Zakkar M, Boyle J, Cuhlmann S, van der Heiden K, Luong le A, Davis J, Platt A, Mason JC, Krams R, Haskard DO, Clark AR, Evans PC. c-Jun N-terminal kinase primes endothelial cells at atheroprone sites for apoptosis. *Arterioscler Thromb Vasc Biol*. 2010;30:546–553. doi: 10.1161/ATVBAHA.109.201368.

18. Heo KS, Lee H, Nigro P, Thomas T, Le NT, Chang E, McClain C, Reinhart-King CA, King MR, Berk BC, Fujiwara K, Woo CH, Abe J. PKCζ mediates disturbed flow-induced endothelial apoptosis via p53 SUMOylation. *J Cell Biol*. 2011;193:867–884. doi: 10.1083/jcb.201010051.
19. Civelek M, Manduchi E, Riley RJ, Stoeckert CJ Jr, Davies PF. Chronic endoplasmic reticulum stress activates unfolded protein response in arterial endothelium in regions of susceptibility to atherosclerosis. *Circ Res*. 2009;105:453–461. doi: 10.1161/CIRCRESAHA.109.203711.
20. Sumi T, Yamashita A, Matsuda S, Goto S, Nishihira K, Furukoji E, Sugimura H, Kawahara H, Imamura T, Kitamura K, Tamura S, Asada Y. Disturbed blood flow induces erosive injury to smooth muscle cell-rich neointima and promotes thrombus formation in rabbit femoral arteries. *J Thromb Haemost*. 2010;8:1394–1402. doi: 10.1111/j.1538-7836.2010.03843.x.
21. Bombeli T, Karsan A, Tait JF, Harlan JM. Apoptotic vascular endothelial cells become procoagulant. *Blood*. 1997;89:2429–2442.
22. Bombeli T, Schwartz BR, Harlan JM. Endothelial cells undergoing apoptosis become proadhesive for nonactivated platelets. *Blood*. 1999;93:3831–3838.
23. Durand E, Scoazec A, Lafont A, Boddaert J, Al Hajzen A, Addad F, Mirshahi M, Desnos M, Tedgui A, Mallat Z. In vivo induction of endothelial apoptosis leads to vessel thrombosis and endothelial denudation: a clue to the understanding of the mechanisms of thrombotic plaque erosion. *Circulation*. 2004;109:2503–2506. doi: 10.1161/01.CIR.0000130172.62481.90.
24. Edfeldt K, Swedenborg J, Hansson GK, Yan ZQ. Expression of toll-like receptors in human atherosclerotic lesions: a possible pathway for plaque activation. *Circulation*. 2002;105:1158–1161.
25. Mullick AE, Soldau K, Kiosses WB, Bell TA 3rd, Tobias PS, Curtiss LK. Increased endothelial expression of Toll-like receptor 2 at sites of disturbed blood flow exacerbates early atherogenic events. *J Exp Med*. 2008;205:373–383. doi: 10.1084/jem.20071096.
26. Mullick AE, Tobias PS, Curtiss LK. Modulation of atherosclerosis in mice by Toll-like receptor 2. *J Clin Invest*. 2005;115:3149–3156. doi: 10.1172/JCI25482.
27. Scheibner KA, Lutz MA, Boodoo S, Fenton MJ, Powell JD, Horton MR. Hyaluronan fragments act as an endogenous danger signal by engaging TLR2. *J Immunol*. 2006;177:1272–1281.
28. Quillard T, Araújo HA, Franck G, Shvartz E, Sukhova G, Libby P. TLR2 and neutrophils potentiate endothelial stress, apoptosis and detachment: implications for superficial erosion. *Eur Heart J*. 2015;36:1394–1404. doi: 10.1093/eurheartj/ehv044.
29. Ferrante G, Nakano M, Prati F, Niccoli G, Mallus MT, Ramazzotti V, Montone RA, Kolodgie FD, Virmani R, Crea F. High levels of systemic myeloperoxidase are associated with coronary plaque erosion in patients with acute coronary syndromes: a clinicopathological study. *Circulation*. 2010;122:2505–2513. doi: 10.1161/CIRCULATIONAHA.110.955302.
30. Sugiyama S, Kugiyama K, Aikawa M, Nakamura S, Ogawa H, Libby P. Hypochlorous acid, a macrophage product, induces endothelial apoptosis and tissue factor expression: involvement of myeloperoxidase-mediated oxidant in plaque erosion and thrombogenesis. *Arterioscler Thromb Vasc Biol*. 2004;24:1309–1314. doi: 10.1161/01.ATV.0000131784.50633.4f.
31. Villanueva E, Yalavarthi S, Berthier CC, et al. Netting neutrophils induce endothelial damage, infiltrate tissues, and expose immunostimulatory molecules in systemic lupus erythematosus. *J Immunol*. 2011;187:538–552. doi: 10.4049/jimmunol.1100450.
32. Tavora FR, Ripple M, Li L, Burke AP. Monocytes and neutrophils expressing myeloperoxidase occur in fibrous caps and thrombi in unstable coronary plaques. *BMC Cardiovasc Disord*. 2009;9:27. doi: 10.1186/1471-2261-9-27.
33. Tanaka H, Sukhova GK, Swanson SJ, Clinton SK, Ganz P, Cybulsky MI, Libby P. Sustained activation of vascular cells and leukocytes in the rabbit aorta after balloon injury. *Circulation*. 1993;88:1788–1803.
34. Raman KG, Gandley RE, Rohland J, Zenati MS, Tzeng E. Early hypercholesterolemia contributes to vasomotor dysfunction and injury associated atherogenesis that can be inhibited by nitric oxide. *J Vasc Surg*. 2011;53:754–763. doi: 10.1016/j.jvs.2010.09.038.
35. Riessen R, Wight TN, Pastore C, Henley C, Isner JM. Distribution of hyaluronan during extracellular matrix remodeling in human restenotic arteries and balloon-injured rat carotid arteries. *Circulation*. 1996;93:1141–1147.
36. Evanko SP, Angello JC, Wight TN. Formation of hyaluronan- and versican-rich pericellular matrix is required for proliferation and migration of vascular smooth muscle cells. *Arterioscler Thromb Vasc Biol*. 1999;19:1004–1013.
37. Hajra L, Evans AI, Chen M, Hyduk SJ, Collins T, Cybulsky MI. The nf-kappa B signal transduction pathway in aortic endothelial cells is primed for activation in regions predisposed to atherosclerotic lesion formation. *Proc Natl Acad Sci U S Am*. 2000;97:9052–9057.
38. Fang Y, Shi C, Manduchi E, Civelek M, Davies PF. Microrna-10a regulation of proinflammatory phenotype in athero-susceptible endothelium in vivo and in vitro. *Proc Natl Acad Sci U S Am*. 2010;107:13450–13455.
39. Hol J, Wilhelmsen L, Haraldsen G. The murine IL-8 homologues KC, MIP-2, and LIX are found in endothelial cytoplasmic granules but not in Weibel-Palade bodies. *J Leukoc Biol*. 2010;87:501–508. doi: 10.1189/jlb.0809532.
40. von Brühl ML, Stark K, Steinhart A, et al. Monocytes, neutrophils, and platelets cooperate to initiate and propagate venous thrombosis in mice in vivo. *J Exp Med*. 2012;209:819–835. doi: 10.1084/jem.20112322.
41. Magid R, Davies PF. Endothelial protein kinase C isoform identity and differential activity of PKCzeta in an athero-susceptible region of porcine aorta. *Circ Res*. 2005;97:443–449. doi: 10.1161/01.RES.0000179767.37838.60.
42. Naruko T, Ueda M, Haze K, van der Wal AC, van der Loos CM, Itoh A, Komatsu R, Ikura Y, Ogami M, Shimada Y, Ehara S, Yoshiyama M, Takeuchi K, Yoshikawa J, Becker AE. Neutrophil infiltration of culprit lesions in acute coronary syndromes. *Circulation*. 2002;106:2894–2900.
43. Soehnlein O. Multiple roles for neutrophils in atherosclerosis. *Circ Res*. 2012;110:875–888. doi: 10.1161/CIRCRESAHA.111.257535.
44. Harlan JM, Killen PD, Harker LA, Striker GE, Wright DG. Neutrophil-mediated endothelial injury in vitro mechanisms of cell detachment. *J Clin Invest*. 1981;68:1394–1403.
45. Libby P. Seeing and sampling the surface of the atherosclerotic plaque: red or white can make blue. *Arterioscler Thromb Vasc Biol*. 2016;36:2275–2277. doi: 10.1161/ATVBAHA.116.308491.
46. Watanabe H, Hattori S, Katsuda S, Nakanishi I, Nagai Y. Human neutrophil elastase: degradation of basement membrane components and immunolocalization in the tissue. *J Biochem*. 1990;108:753–759.
47. Carden D, Xiao F, Moak C, Willis BH, Robinson-Jackson S, Alexander S. Neutrophil elastase promotes lung microvascular injury and proteolysis of endothelial cadherins. *Am J Physiol*. 1998;275:H385–H392.
48. Yang JJ, Kettritz R, Falk RJ, Jennette JC, Gaido ML. Apoptosis of endothelial cells induced by the neutrophil serine proteases proteinase 3 and elastase. *Am J Pathol*. 1996;149:1617–1626.
49. Dinerman JL, Mehta JL, Saldeen TG, Emerson S, Wallin R, Davda R, Davidson A. Increased neutrophil elastase release in unstable angina pectoris and acute myocardial infarction. *J Am Coll Cardiol*. 1990;15:1559–1563.
50. Saffarzadeh M, Juenemann C, Queisser MA, Lochnit G, Barreto G, Galuska SP, Lohmeyer J, Preissner KT. Neutrophil extracellular traps directly induce epithelial and endothelial cell death: a predominant role of histones. *PLoS One*. 2012;7:e32366. doi: 10.1371/journal.pone.0032366.
51. Carmona-Rivera C, Zhao W, Yalavarthi S, Kaplan MJ. Neutrophil extracellular traps induce endothelial dysfunction in systemic lupus erythematosus through the activation of matrix metalloproteinase-2. *Ann Rheum Dis*. 2015;74:1417–1424. doi: 10.1136/annrheumdis-2013-204837.
52. Mangold A, Alias S, Scherz T, et al. Coronary neutrophil extracellular trap burden and deoxyribonuclease activity in ST-elevation acute coronary syndrome are predictors of ST-segment resolution and infarct size. *Circ Res*. 2015;116:1182–1192. doi: 10.1161/CIRCRESAHA.116.304944.
53. Stakos DA, Kambas K, Konstantinidis T, Mitroulis I, Apostolidou E, Arelaki S, Tsironidou V, Giatromanolaki A, Skendros P, Konstantinides S, Ritis K. Expression of functional tissue factor by neutrophil extracellular traps in culprit artery of acute myocardial infarction. *Eur Heart J*. 2015;36:1405–1414. doi: 10.1093/eurheartj/ehv007.
54. Jia H, Dai J, Hou J, Xing L, Ma L, Liu H, Xu M, Yao Y, Hu S, Yamamoto E, Lee H, Zhang S, Yu B, Jang IK. Effective anti-thrombotic therapy without stenting: Intravascular optical coherence tomography-based management in plaque erosion (the EROSION study). *Eur Heart J*. 2017;38:792–800. doi: 10.1093/eurheartj/ehw381.
55. Libby P. Superficial erosion and the precision management of acute coronary syndromes: not one-size-fits-all. *Eur Heart J*. 2017;38:801–803. doi: 10.1093/eurheartj/ehw599.

Circulation Research
JOURNAL OF THE AMERICAN HEART ASSOCIATION

Flow Perturbation Mediates Neutrophil Recruitment and Potentiates Endothelial Injury via TLR2 in Mice: Implications for Superficial Erosion

Grégory Franck, Thomas Mawson, Grasiele Sausen, Manuel Salinas, Gustavo Santos Masson, Andrew Cole, Marina Beltrami-Moreira, Yiannis Chatzizisis, Thibault Quillard, Yevgenia Tesmenitsky, Eugenia Shvartz, Galina K. Sukhova, Filip K. Swirski, Matthias Nahrendorf, Elena Aikawa, Kevin J. Croce and Peter Libby

Circ Res. 2017;121:31-42; originally published online April 20, 2017;
doi: 10.1161/CIRCRESAHA.117.310694
Circulation Research is published by the American Heart Association, 7272 Greenville Avenue, Dallas, TX 75231

Print ISSN: 0009-7330. Online ISSN: 1524-4571

SUPPLEMENTAL MATERIAL

Material and Methods

Human atheromata selection: Human specimens of carotid plaques were obtained after endarterectomy (n = 146) by protocols approved by the Human Investigation Review Committee at the Brigham and Women's Hospital. We used morphologic criteria to categorize plaques as "erosion prone" (SMC-rich, macrophage-poor, high apoptotic luminal EC content; 15.3 ± 4.8 $TUNEL^+$ EC per field, n=7), "stable fibrous" (SMC-rich, macrophage-poor, low apoptotic luminal EC content; 3 ± 0.6 $TUNEL^+$ EC per field, n=10, p=0.0014), or "eroded" (SMC-rich, macrophage-poor, non-obstructive mural thrombus, n=8). Atheromata with features associated with fibrous cap rupture (few SMC, many macrophages, large lipid core, n=11) was used as a control group. Damage tissues (n=49), calcified nodules or other morphologies (n=40) were excluded from the study. Two investigators independently performed the analysis and classification of the tissue specimens.

Animals: C57B6 Apolipoprotein-E deficient mice (*Apoe*$^{-/-}$) and Toll-like receptor 2 deficient mice (TLR2$^{-/-}$) male mice (Jackson Laboratories, USA), 8–12 weeks of age, were housed in the Harvard Medical School Facilities at the New Research Building (Boston, MA, USA) and consumed a normal chow diet with water ad libitum. Mice were certified free of common pathogens by the suppliers and were monitored by the Harvard Medical Area Standing Committee on Animals. Double compound *Apoe*$^{-/-}$*Tlr2*$^{-/-}$ were generated in house. Genotyping for both *Apoe*-/- and *Apoe*-/-TLR2 mice was performed routinely by tail biopsies (**Supplementary Fig. IIIf**). Sample size was determined according to pilot experiments.

Arterial injury: The protocol described below resulted from optimization by extensive pilot experiments. Eight-week-old *Apoe*$^{-/-}$ mice underwent electrical injury of the left common carotid artery (LCCA) as previously described[1] to produce an intimal lesion rich in smooth muscle cells and in proteoglycan and glycosaminoglycans including hyaluronan (**Fig. 1**). Briefly, the left common carotid artery (LCCA, 500 ± 20 μm diameter) was exposed by an incision on the ventral side of the neck. LCCA was injured by electric current using a bipolar microcoagulator (Erbe ICC 200, USA) delivered through the tips of microforceps positioned perpendicularly to the longitudinal axis of the artery. A uniform injury was induced by applying a current pulse two times every millimeter from beneath the LCCA bifurcation. The total injured distance encompassed approximately 2 mm, depending on the anatomical

variability of the artery. A current pulse of 3W was delivered by the microcoagulator for 4s each time. Such pulses resulted in reproducible neointima formation (**Fig. 1b,c**), whose features mimicked the morphologic and the biochemical characteristics of human atheromata that have produced thrombosis to superficial erosion [2,3]. Left common carotid arteries served as uninjured controls.

In vivo flow perturbation: Four weeks after arterial injury (12-week-old mice), the intima had healed and re-endothelialization was complete (**Fig. 1a**). Local flow perturbation was induced either in normal LCCA or in the previously injured LCCA. This procedure used polyethylene cuffs custom manufactured to our specifications by 3D-stereolithography printing (Proto Labs, USA) that form a cone-shaped lumen and produce vortices downstream when placed and fixed with a 7-0 Ethilon nylon suture (Ethicon) around the artery (**Fig. 2**). The non-constrictive proximal internal diameter (500 μm) of the cuff decreases gradually to become constrictive at its end (distal internal diameters: 250 μm). Blood flow in both the pre- and post-stenotic region was monitored during cuff placement and its perturbation was assessed by Doppler-coupled ultrasonography (VisualSonics 2100). Animals that underwent a sham procedure (with no cuff placement) and those that had placement of a non-constrictive device served as controls for the surgical manipulations and for adventitial injury and inflammation.

Computational fluid dynamics: Geometry, Mesh Construction, and Simulation Set-up: Computational fluid dynamics using finite volume analysis verified the extent of flow perturbation, recirculation, and the presence of oscillatory shear stress distal to the constrictive cuff. Using previously injured vessels, the LCCA geometry with or without cuff placement was virtually constructed using Ansys DesignModeler (Ansys Inc., Canonsburg, USA). Each mesh was built with 1.3×10^6 elements and 2.7×10^5 nodes and imported into the CFX CFD solver (CFX version 15.0, Ansys Inc., Canonsburg, USA). At the inlet, a normalized transient velocity waveform boundary condition was prescribed, representing the vessel flow velocity measured by Doppler-coupled ultrasonography. The outlet was set to zero relative-pressure, and no-slip conditions were imposed at the vessel walls. All simulations utilized a Newtonian, viscous model, with laminar flow conditions with the following fluid material properties: density = 1.025g/cm3 and dynamic viscosity = 3.5 cp (Windberger *et al*. 2003). A convergence criteria of 1×10^{-9} was reached for the momentum and continuity equations. Simulations were conducted in a Hewlett Packard workstation with intel(R) Xeon(R) CPU, x5550@ 3.67GHz (6 processors) with 32.0 GB installed memory and

64-bit windows 8 operating system. Data post-processing was performed through Tecplot (Tecplot Inc., Bellevue, USA).

In vivo TLR2 activation: 8-10-week-old mice received a potent TLR2 agonist, Pam3CSK4 (1mg/kg i.p., InvivoGen), a synthetic endotoxin-free triacylated lipopeptide that mimics the acylated amino terminus of bacterial LPS. After 6h, injected mice were euthanized and their arteries were used for further QPCR or western blot experiments.

Biological analysis: Flow perturbation was conducted for 1 or 6 hours and mice were euthanized by CO_2 inhalation and bilateral thoracotomy. Peripheral blood sampling was performed and mice were perfused with cold PBS using intracardiac perfusion, then fixed with 4% paraformaldehyde. Distal and proximal LCCA samples were collected and embedded in optimal cutting temperature medium (OCT). Six µm cryo-tome sections were prepared and stained for immunohistochemistry/immunofluorescence investigation.

Immunohistochemistry / Immunofluorescence: Immunostaining on frozen cross sections was performed using rat monoclonal anti-mouse Ly6G (Santa Cruz Biotechnologies) and rat monoclonal anti-mouse CD31 (BD Pharmingen). Vessels showing total occlusion or aneurysmal features were excluded from the analysis. This criterion was pre-established. After incubation with a biotin-conjugated anti-rat antibody (Vector Laboratories), immunostaining was amplified using peroxidase-conjugated streptavidin complexes (Vector Laboratories) and peroxidase was detected using AEC (Vector Laboratories) substrate. Sections were lightly counterstained with hematoxylin, mounted in gelatin glycerol and examined with a bright field microscope (Nikon Optiphot-2 equipped with a Nikon digital camera DXM 1200F). For double immunostaining study, cross sections were incubated with primary antibodies followed by the incubation with a fluorophore-coupled anti-species antibody (Life Technologies), stained with DAPI, and mounted with a fluorescent mounting medium (DAKO). Slides were kept in the dark at 4°C. **For thrombus formation, Carstairs staining (Electron Microscopy Sciences, USA) was performed according to manufacturer's protocol. The fibrinogen immunostaining used a goat anti-fibrinogen antibody (SantaCruz) and was performed on serial sections of carotid sections subjected to flow perturbation after 1 and 6 hours.**

Endothelial permeability: Endothelial permeability was investigated by monitoring extravasation of Evan's Blue dye (EBD). The blue staining of EBD-albumin conjugate was evident in LCCA sections subjected to injury (**Fig. 1**) and/or flow perturbation (**Fig. 4**). Mice were injected after electric injury or 6 hours after flow perturbation, via retro-orbital injection

of 50 µL of 7% EBD (Sigma). After 10 min, mice were euthanized by CO_2 inhalation, perfused by left ventricular apical cannulation with PBS at 4°C supplemented with heparin 10U/ml, and were then fixed with a perfusion of 10% formalin. LCCA was embedded in OCT and kept at -80°C for histology. Whole LCCA was carefully harvested, opened longitudinally from the aortic arch to the bifurcation and stabilized on glass with hardening mounting medium (Vector, Vecta Mount H-5000). In some mice, the LCCA served as a control. Arteries were examined by bright field imaging.

Neutropenia and neutralization of neutrophil recruitment: Circulating neutropenia was induced 24 hours before experiments using a single injection i.v of anti-Ly6G blocking monoclonal antibody (300µg, Clone RB6-8C5, BioXCell) in a total of 300µl in sterile saline as diluent. Neutralization of neutrophil recruitment was performed with a single injection i.v of anti-LFA-1 blocking monoclonal antibody 1h before experiments (150µg, Clone I21/7, ThermoScientific). Control animals were injected with saline 1h before experiment.

Electron microscopy: Samples (injured LCCA subjected to flow after 1 or 6h, or injured LCCA with no flow, n=3) were isolated and immediately placed in fixative solution (Formaldehyde/Glutaraldehyde, 2.5% each in 0.1M sodium cacodylate buffer, pH 7.4) overnight. Ultrathin sections of 70 to 80 nm were cut on a Reichert Ultracut-S, stained with 2% uranyl acetate and viewed using a JEOL 1200EX transmission electron microscope equipped with an AMT 2k CCD camera.

En face microscopy: The mouse vasculature was fixed with a perfusion of cold 4% PFA. The carotids (n=3 per group) were dissected and longitudinally opened on a sylgard dish and extensively fixed in 4% PFA for 48-72h. Fixation was quenched with 100 mM glycine (pH 7.4), and carotids were washed extensively in PBS. Arteries were permeabilized and treated with a blocking buffer containing 5% NGS, 1%BSA and 0.05% Triton X-100 during 2 h at room temperature. Primary antibodies were diluted in blocking buffer and incubated with carotid artery specimens for 48 h at 4°C. Tissues were washed in PBS, then washed in blocking buffer for 2 h. The carotids were incubated 1 h at room temperature, with fluorophore-conjugated antibodies diluted in blocking buffer. Finally, the tissues were washed in blocking buffer for 1 h at room temperature, then washed in PBS. Primary antibodies used included: CD31 (BD Pharmingen), Ly6G (Santa Cruz Biotechnologies), citrullinated Histone H3 (Abcam), and Myeloperoxidase (Abcam). Secondary antibodies (Life Technologies) were all conjugated with Alexa-Fluor 488 or 555. All preparations were mounted with Vectashield

HardSet Antifade Mounting Medium containing DAPI for DNA staining (Vector Laboratories) and stored in the dark at room temperature.

Bone marrow transplantation: Apoe$^{-/-}$ or *Apoe*$^{-/-}$*Tlr2*$^{-/-}$ male C57B6 mice served as recipients for transplantation (6-8 week old). Recipient mice received 1,050 rads of split-dosed lethal irradiation (5.25 Gy, twice) 4 h apart to reduce gastrointestinal toxicity. Recipient mice received antibiotics (sulfamethoxazole and trimethoprim, HiTech Parmacal) until the end of the experiment. Total bone marrow cells from *Apoe*$^{-/-}$ or *Apoe*$^{-/-}$*Tlr2*$^{-/-}$ donor mice were prepared from the femurs and tibias collected aseptically in sterile RPMI 1640 medium supplemented with 2% FBS, 10 U/ml heparin, penicillin and streptomycin. Bones were punched with a needle at both of their extremities and centrifuged using a mounting of modified sterile tubes (**Supplementary Fig. Vb**). Cells were resuspended and washed twice in sterile serum-free RPMI 1640 medium supplemented with 20mM HEPES, penicillin and streptomycin at pH 7.4. After counting, 5 million total bone marrow cells were injected i.v into each recipient mouse (6-week-old) for reconstitution. Mice with no bone marrow reconstitution served as sentinels. Mice were monitored until the final experiments, and survival curves were established for each group (**Supplementary Fig. Va**).

RNA isolation: For EC peeling, carotids were isolated, rinsed with cold PBS, and flushed with 1ml of Trizol reagent (ThermoFisher Scientific) using syringe 27 gauge (BD). After chloroform addition, total RNA extraction was performed using PureLink Micro kit (Life Technologies) according to manufacturer's instructions. For whole arteries, carotid samples or aortas were ground to a fine powder in liquid nitrogen and total RNA was extracted in Trizol reagent and PureLink RNA Micro kit. The purity and concentration of total extracted RNA was evaluated using a spectrophotometer (NanoDrop). The RNA was reverse transcribed using the SuperScript II reverse transcriptase (Invitrogen). The resulting cDNA mixture was stored at -80°C until further use.

Quantitative PCR: The mRNA levels of 15 candidate genes (**Supplementary Table 1**) were determined by quantitative real-time-polymerase chain reaction (QRT-PCR) using a CFX Connect™ Real-Time PCR Detection System (Bio-Rad) using SsoAdvanced Universal SYBR Green Supermix (Bio-Rad). Amounts of mRNA of interest were normalized to that of βActin (ΔCt = Ct gene of interest - Ct βActin). Analysis was performed using the $2(-\Delta Ct)$ or $2(-\Delta\Delta Ct)$ method.

Immunoblotting: Samples were macerated on ice and lysates were prepared with ice-cold RIPA buffer (Boston BioProducts, USA) supplemented with proteases inhibitors (Complete

Mini, Roche). Lysates were separated by SDS-PAGE and transferred to polyvinylidene difluoride membranes. The membranes were probed overnight with primary antibodies and anti-β-actin antibody at 4°C. After incubation with horseradish peroxidase-linked secondary antibodies (ThermoFisher Scientific), immunoreactive proteins were visualized with an ultra-sensitive enhanced chemiluminescent substrate (ThermoFisher Scientific, USA).

ELISA: Peripheral blood was collected and levels of circulating fibrin byproduct D-dimer and neutrophil chemoattractant KC were evaluated using commercially available ELISA kits (NeoBiolab and Promokine, respectively).

Flow cytometry: After harvesting, carotid arteries were gently washed with cold PBS solution supplemented with 5% BSA and minced with surgical scissors. Single-cell suspension was obtained through enzymatic digestion in collagenase I (450 U/ml), collagenase XI (125 U/ml), DNase I (60 U/ml), and hyaluronidase (60 U/ml) (Sigma-Aldrich, St. Louis, MO, USA) at 37°C on a shaker set at 750 rpm for 1 hour. Samples were filtered with a 40 μm cell strainer and stained with the following anti-mouse biotinylated antibodies (1:600 dilution) against lineage (Lin) markers: B220 (Biolegend, clone RA3-6B2), NK1.1 (Biolegend, clone PK136), Ter119 (Biolegend, clone TER-119), CD90 (Biolegend, clone 53-2.1), IL7Rα (Biolegend, clone A7R34), CD4 (Biolegend, clone GK1.5) and CD8 (BD Biolegend, clone 53-6.7). After the lineage staining, single-cell suspension was stained with the following antibodies (1:600 dilution): Brilliant Violet 711 anti-mouse CD45 (Biolegend, clone A20), PE/Cy7 anti-mouse F4/80 (Biolegend, clone BM8), PE/Cy5 anti-mouse Ly6G (Biolegend, clone 1A8), Brilliant Violet 605 anti-mouse Ly6C (Biolegend, clone HK1.4), APC anti-mouse/human CD11b (Biolegend, clone M1/70), and Brilliant Violet 510 Streptavidin (Biolegend). Viability was assessed using the Fixable Viability Dye eFluor 780 (eBioscience). Live neutrophils were identified as Lin-CD45+CD11b+LY6G+.

For the quality control of the chimeric mice 4 weeks after bone marrow reconstitution, 100 μl of blood was collected through eye bleeding. Samples were incubated with RBCs lysis buffer (Biolegend) for 2 minutes at room temperature and stained with biotin anti-mouse CD90 (Biolegend, clone 30-H12). Samples were later incubated with the following anti-mouse antibodies: FITC LY6C (Biolegend, clone HK1.4), CD115 PERCP (Biolegend, clone AFS98), CD19 PE/Cy7 (Biolegend, clone 6D5), APC LY6G (Biolegend, clone 1A8), APC/Cy7 CD11b (Biolegend, clone M1/70), PE TLR2 (Biolegend, clone CB225), and Brilliant Violet 605 Streptavidin (Biolegend, clone). Neutrophils were identified as CD90-CD19-CD115-CD11b+LY6G+ cells. Bone marrow chimerism was assessed as percentage of

TLR2+ or - neutrophils. We acquired data on an LSRII flow cytometer (BD Bioscience) with FACSDiva software (BD Bioscience). Experimental data were analyzed using FlowJo software (Tree Star Inc.).

Cell culture: Human saphenous vein EC (HSVEC) were isolated from saphenous veins enzymatically, and cultured on 1% gelatin-coated dishes in Medium 199 (Lonza) supplemented with 20% fetal bovine serum (FBS), penicillin/streptomycin, L-glutamine, heparin, and 0.05mg/ml ECGS (Alfa Aesar) between passages 2 and 5. After reaching confluence, HSVECs were deprived with OptiMEM medium (ThermoFisher) supplemented with 3% FBS for 6 to 12 hours before activation by TLR2 agonists Pam3csk4 (Pam3, 2µg/ml) for the indicated times (Invivogen). Alternatively, EC were seeded on a HA-supplemented gelatin coating with selected molecular weight (HA, Lifecore Biomedical). Cell lysates were prepared after 48 hours for RNA isolation. Cultured HSVECs were previously authenticated by morphology, and the assessment of the expression of von Willebrand Factor by immunofluorescence and QPCR[4].

Acquisition and morphometric analysis: In situ images were captured digitally using a BX61WI microscope coupled with a Fluoview FV1000 confocal unit (Olympus) equipped with an Olympus DP72 camera and running Fluoview 10-ASW Software (Olympus) for confocal microscopy or a Nikon Optiphot-2 equipped with a Nikon digital camera DXM 1200F for bright field microscopy. Macroscopic images were taken using the confocal apparatus and Cell Sens software (Olympus). The number of Ly6G-positive cells, CD31-positive cells, $CD31^{+}TUNEL^{+}$ cells, endothelium continuity, and Evans blue coverage were quantified after an immunostaining computer-assisted method (Image-Pro Plus, Media Cybernetics) and using a double-blind randomized approach.

Statistics: Animals were randomly allocated to treatment or control groups. Investigator was blinded to the group allocation during the experiment. Data were analyzed to assess normality of distribution. A non-parametric test was used for skewed data. For normally-distributed variables, data were expressed as mean ± SEM and analyzed by the t-test, Mann-Whitney or Kruskal–Wallis one-way analysis of variance and Dunn's post (GraphPad Prism, USA). Differences were considered statistically significant at the $p<0.05$ level (unadjusted p values). Correlation was estimated with Pearson product-moment.

References

1. Carmeliet, P.*, et al.* Vascular wound healing and neointima formation induced by perivascular electric injury in mice. *The American journal of pathology* **150**, 761-776 (1997).
2. Virmani, R., Kolodgie, F.D., Burke, A.P., Farb, A. & Schwartz, S.M. Lessons from sudden coronary death: a comprehensive morphological classification scheme for atherosclerotic lesions. *Arteriosclerosis, thrombosis, and vascular biology* **20**, 1262-1275 (2000).
3. Falk, E., Nakano, M., Bentzon, J.F., Finn, A.V. & Virmani, R. Update on acute coronary syndromes: the pathologists' view. *European heart journal* **34**, 719-728 (2013).
4. Libby, P., Ordovas, J.M., Birinyi, L.K., Auger, K.R. & Dinarello, C.A. Inducible interleukin-1 gene expression in human vascular smooth muscle cells. *The Journal of clinical investigation* **78**, 1432-1438 (1986).

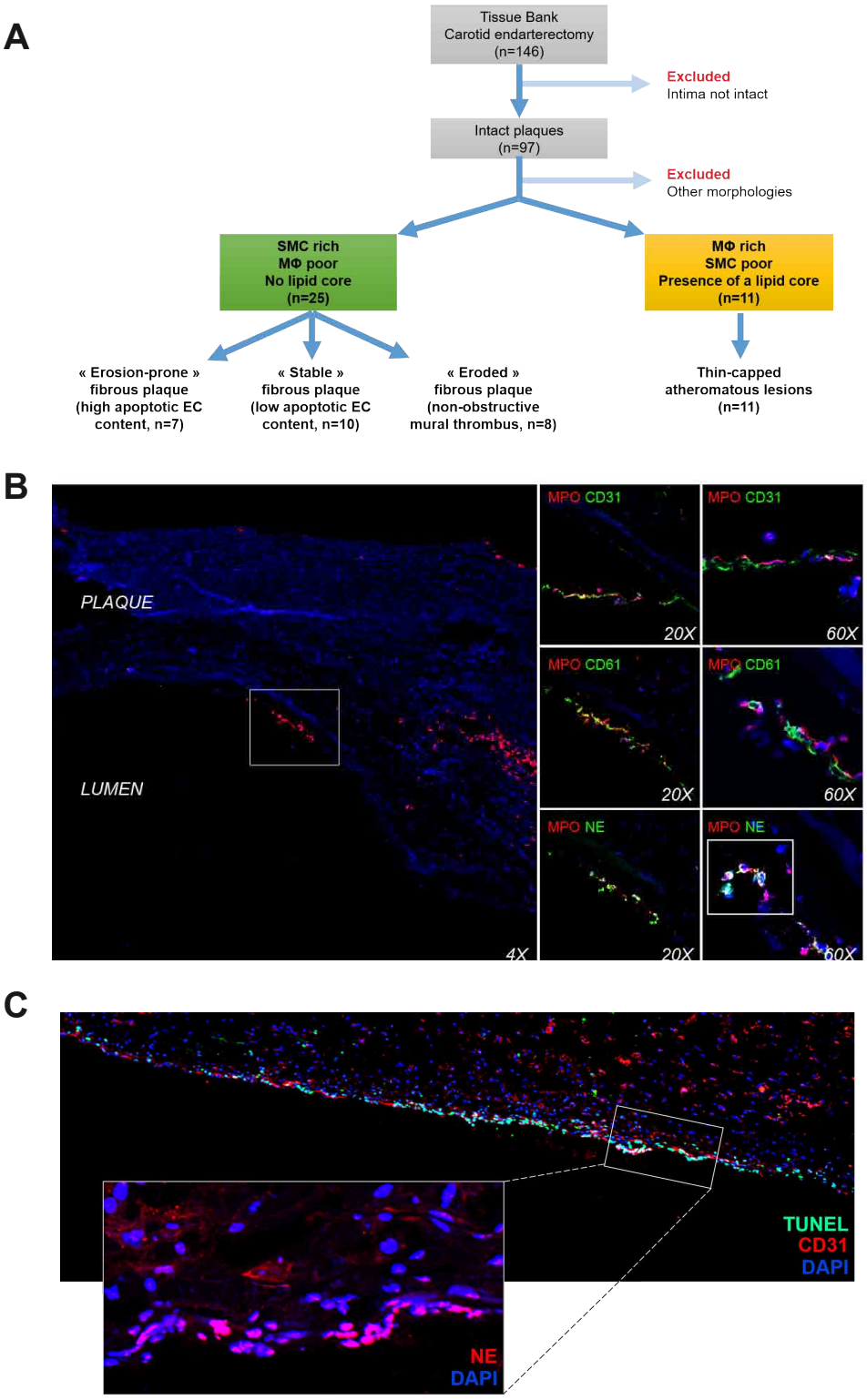

Figure I: Characterization of human endaractomy samples. (**A**) Screening of the sample was performed after classifying plaques as SMC-rich, macrophage-poor, without lipid cores (n=25) or macrophage-rich, SMC-poor with the presence of a lipid core (n=11). The first group was divided into “Erosion-prone” fibrous plaque (high apoptotic EC content, n=7), “stable” fibrous plaque (low apoptotic EC content, n=10) or “Eroded” fibrous plaques (presence of a non-obstructive mural thrombi, n=8). The second group (yellow) classified the thin-capped atheromatous lesions. (**B**) Immunofluorescent labeling of neutrophils, platelets, myeloperoxidase, and neutrophil elastase in a human plaque with erosion-prone characteristics obtained at carotid endarterectomy. (**C**) Immunostaining showing luminal TUNEL positive cells in contiguity with neutrophil elastase-bearing cells in a human plaque with erosion-prone characteristics obtained at endarterectomy

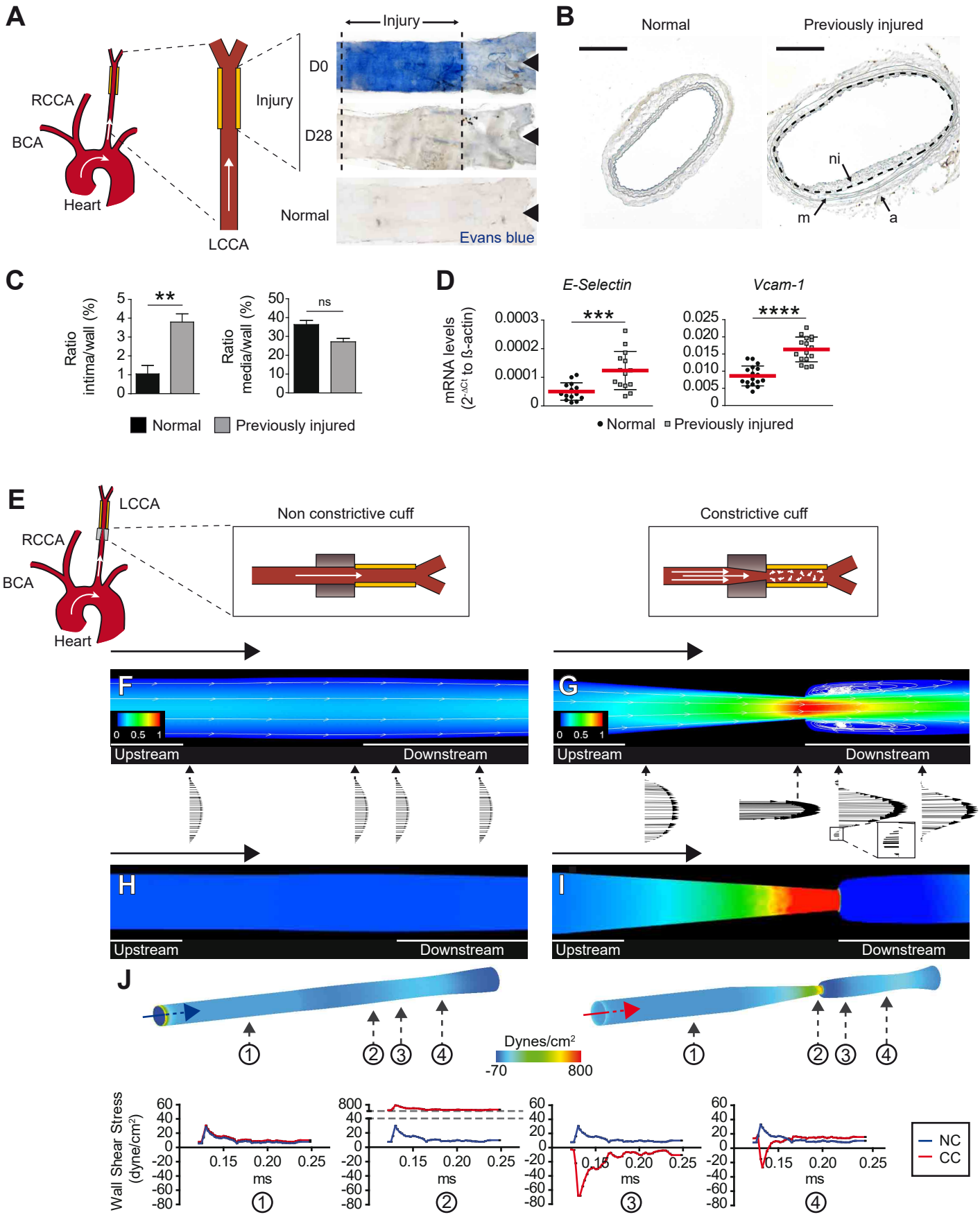
A
RCCA
BCA
Heart
LCCA
Injury
D0
D28
Normal
Evans blue
B
Normal
Previously injured
ni
m
a
C
Ratio intima/wall (%)
**
Ratio media/wall (%)
ns
Normal
Previously injured
D
E-Selectin
Vcam-1
mRNA levels (2^-ΔCt to β-actin)
***
****
Normal
Previously injured
E
LCCA
RCCA
BCA
Heart
Non constrictive cuff
Constrictive cuff
F
G
H
I
Upstream
Downstream
J
Dynes/cm²
-70
800
Wall Shear Stress (dyne/cm²)
ms
NC
CC

Figure II Creation of an experimental substrate for probing superficial erosion in mice. (**A**) Experimental protocol showing carotid electric injury (yellow segment) performed at day 0 and followed after 4 weeks by completed endothelial reconstitution assessed by an Evans blue staining. The arrow represents flow orientation. (**B**) H&E staining shows the formation of a neointima in carotid subjected to injury. ni: intima, m: media, a: adventitia, dashed line: internal elastic laminae. Scale bars, 200 μm. (**C**) Quantification of the ratio intima/wall (left) and the ratio media/wall (right) in normal arteries vs previously injured arteries. **p<0.01, ns, non-significant. QPCR analysis was performed on normal vs previously injured carotid for the expression of endothelial adhesion molecules (**D**). Data are expressed in $2^{-\Delta Ct}$ to β-actin. Each dot represents data from one animal. (**E**) Placement of a cone-shape polyethylene cuff around the RCCA in mice and secured by a circumferential suture. Non-constrictive control cuff (**F**) or constrictive cuff (**G**) effect on blood flow perturbation in carotid arteries. Doppler-coupled ultrasonography showing velocity patterns along the downstream flow (left, arrow) and the velocity peak downstream of the cuff (right, arrow) measured at 1.5 mm downstream of the cuff (arrowhead). Computational fluid dynamics using finite volume analysis verified the extent of flow perturbation, recirculation, and the presence of oscillatory shear stress distal to the constrictive cuff. Longitudinal cross-sectional simulation of the effect of a non-constrictive cuff (**F,H**) or a constrictive cuff (**G,I**) showing a normalized axial velocity contour with superimposed velocity vectors (**F,G**) or showing a normalized shear stress contour (**H,I**). (**J**) Time averaged wall shear stress plots measured after the placement of non-constrictive (blue line) vs constrictive cuff (red line) at identical locations: (1) upstream from the cuff, (2) narrowest cuff point, (3) slightly downstream from the cuff, (4) further downstream from the cuff. RCCA: right common carotid artery, LCCA: left common carotid artery, BCA: Brachiocephalic artery, ECA: external carotid artery, ICA: internal carotid artery, NC: non-constrictive cuff, CC: constrictive cuff. Data are expressed in Dynes/$cm^{2.}$

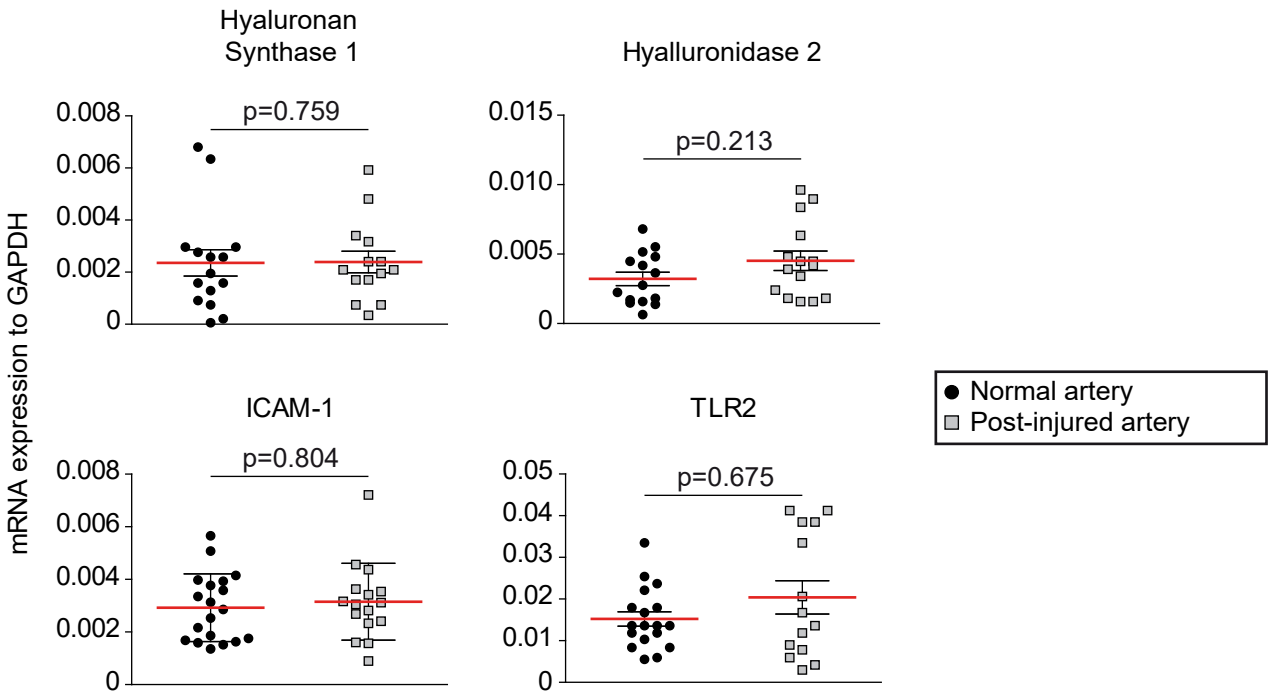

Figure III Gene expression in carotids after electric injury. mRNA expression of Hyaluronan Synthase 1, Hyalluronidase 2, Interecellular adhesion molecule 1 (ICAM-1) and Toll-like recepteur 2 (TLR2).

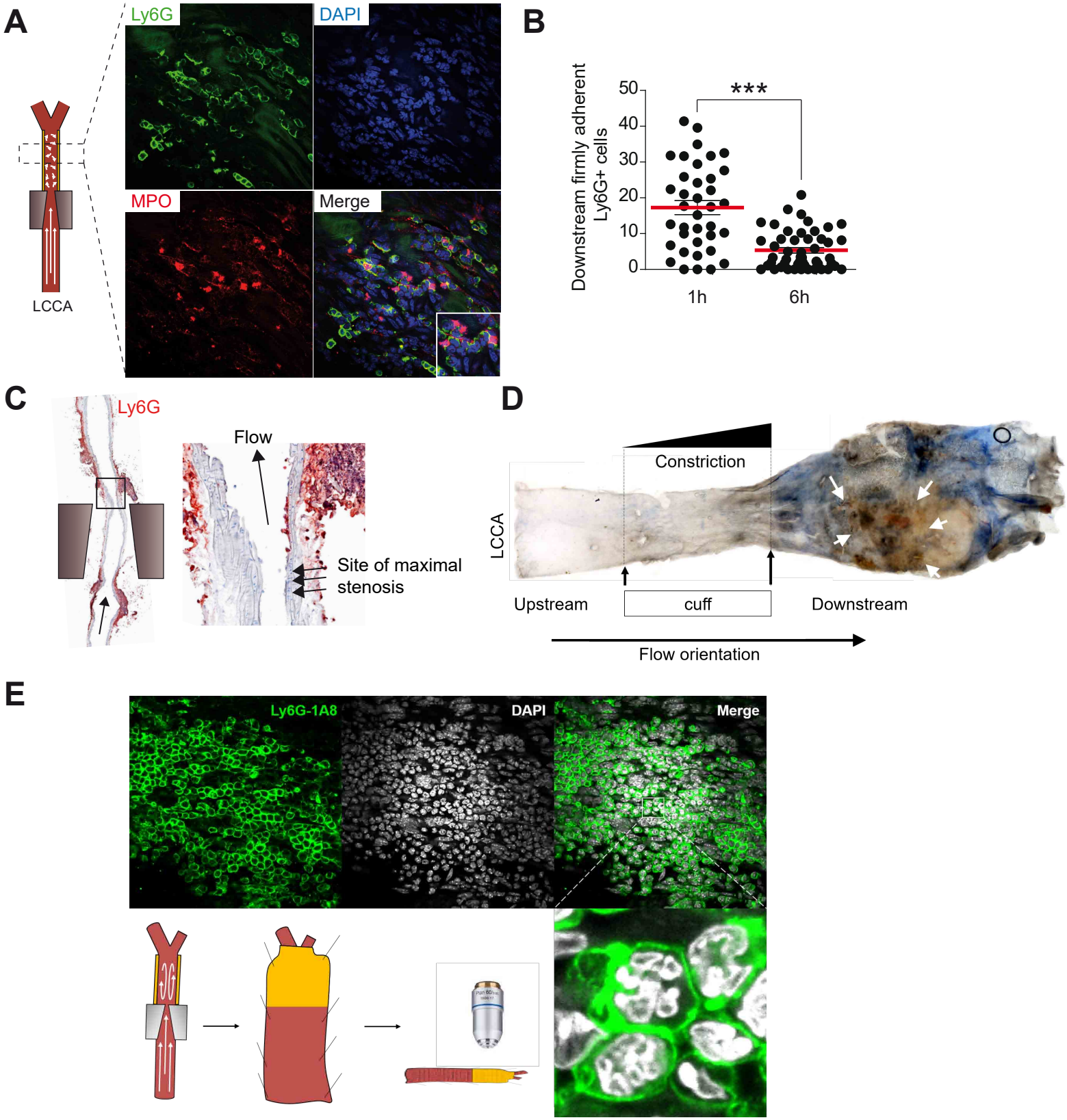

Figure IV Recruited neutrophils during flow perturbation and localization of thrombus. (**A**) Colocalization in immunofluorescence and en face visualization show the expression of MPO by Ly6G$^+$ and Ly6G$^-$ cells. Quantification of downstream firmly adherent Ly6G$^+$ cells 1 and 6h after flow perturbation, ***p<0.001. (**B**) Ly6G staining on a longitudinal section showing the site of maximal stenosis, devoid of neutrophil, and neutrophil accumulation downstream. (**C**) Localization of thrombus formation in the mouse carotid artery after flow perturbation. The carotid was opened for an en face visualization of the intima. Cuff position is notified with the black arrows. The blue indicates EC permeability to Evans Blue dye, whereas the brown color shows accumulation of erythrocyte-enriched fresh thrombus. (**D**) En face immunofluorescent observation of adherent neutrophils in the mouse carotid after flow perturbation using the anti-Ly6G clone 1A8 antibody. LCCA: left common carotid artery.

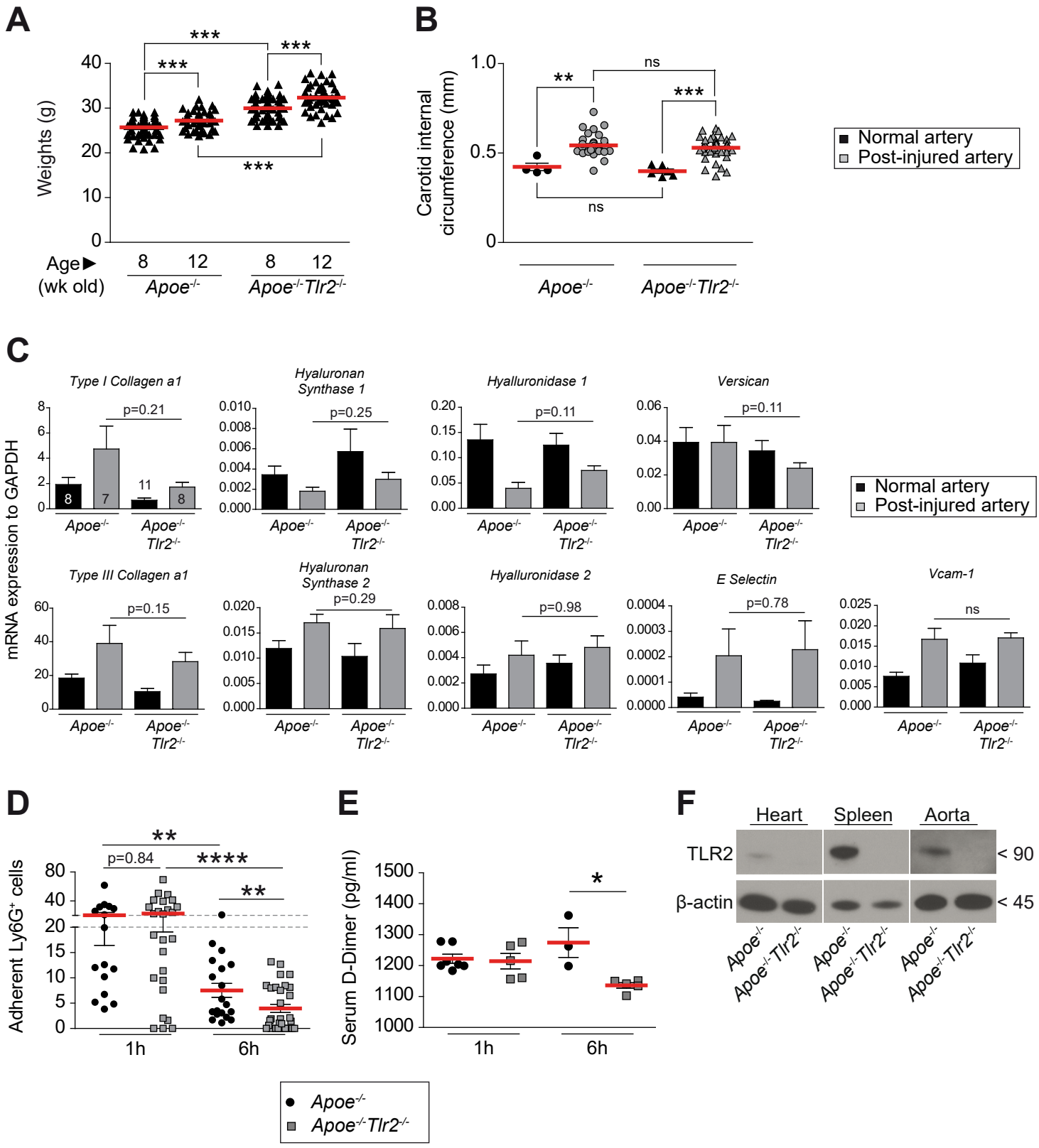

Figure V Effect of Tlr2 knock out on weight, arterial composition and neutrophil recruitment.

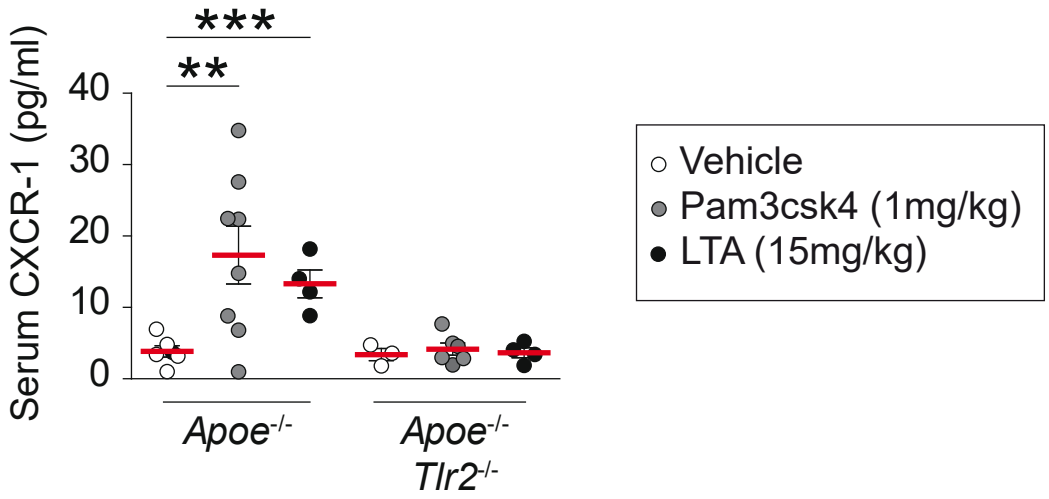

Figure VI Effect of a systemic injection of two different TLR2 agonists on the levels of circulating CXCR-1

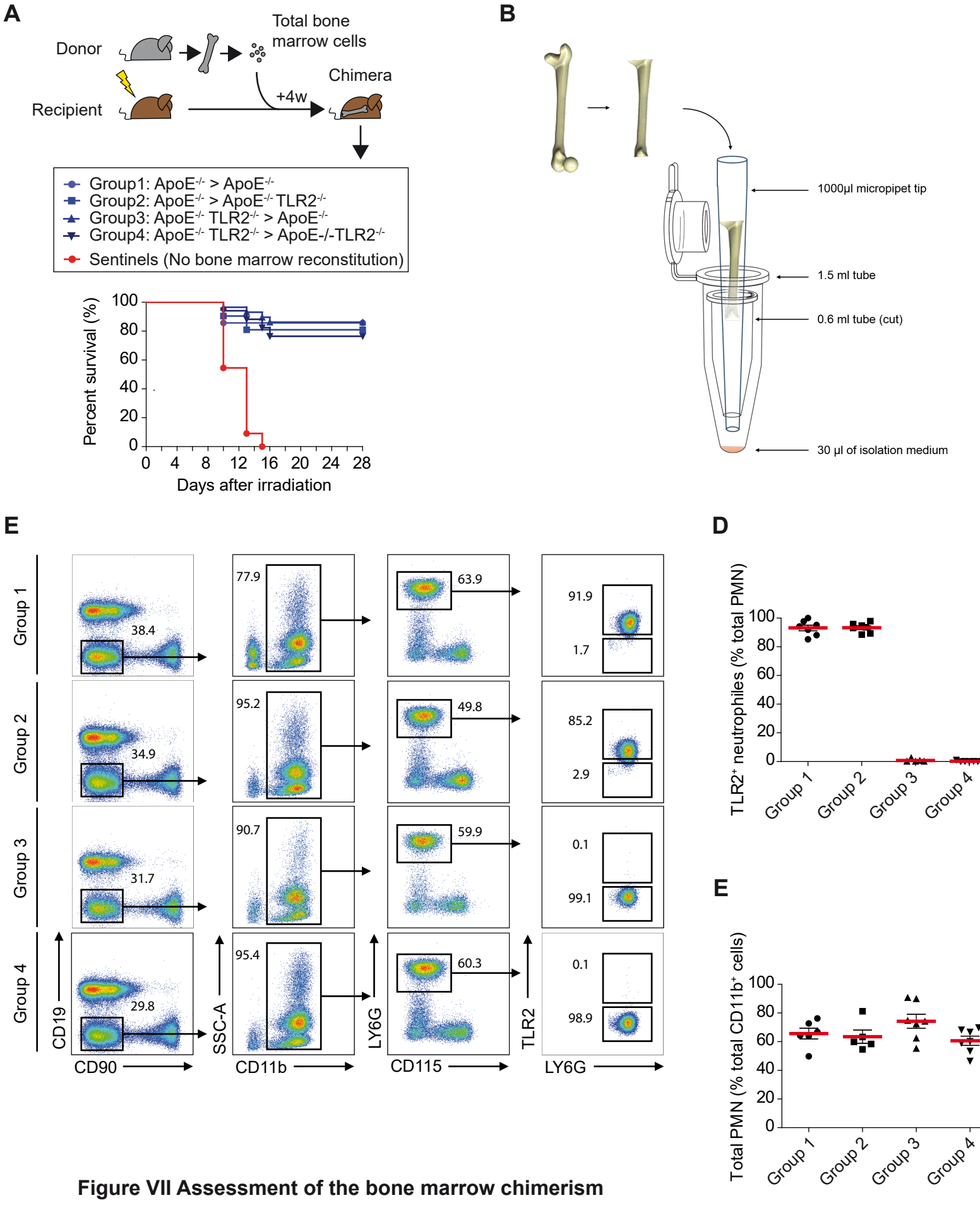

Figure VII Assessment of the bone marrow chimerism

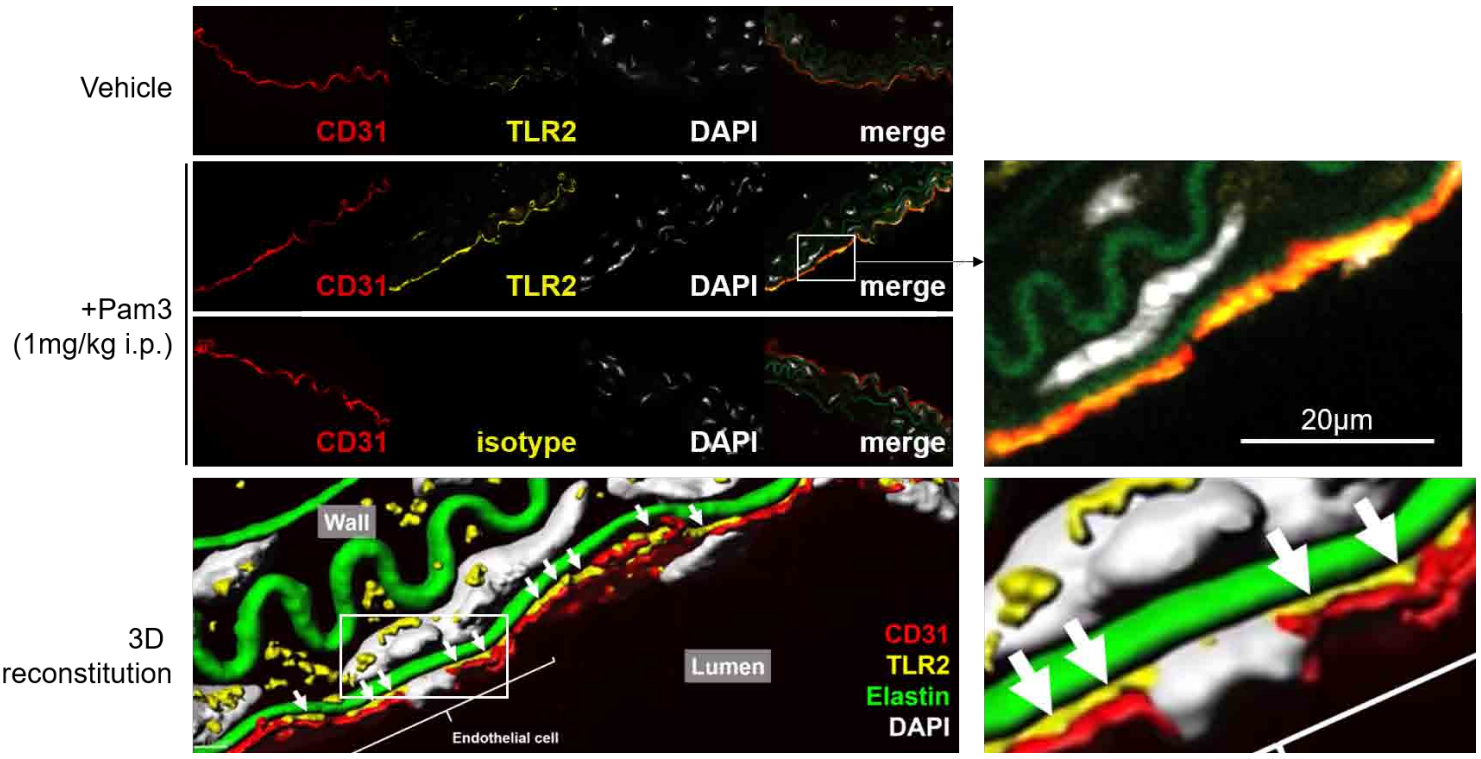

Figure VIII Expression of TLR2 by ECs in the mouse carotid. Immunofluorescence images show the over-expression of TLR2 by EC (CD31) in Pam3-treated mice (**upper panel**). 3D reconstituation of the 10µm thick section showing a basal localization of TLR2 expressed by luminal ECs (**lower panel**).

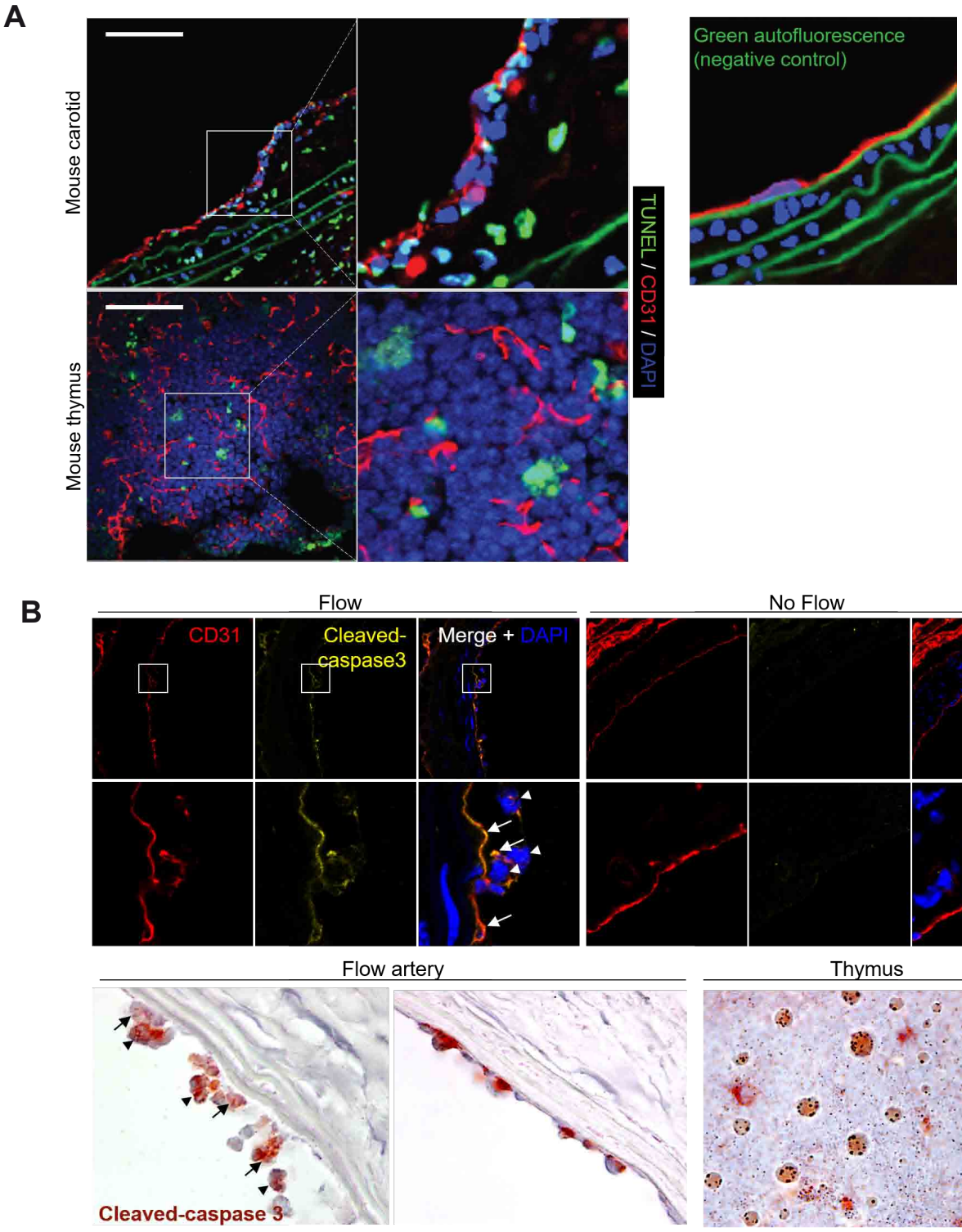

Figure IX Immunofluorescence and immunoflhistochemistry assesment of apoptosis. (**A**) Immuno-fluorescent staining TUNEL/CD31 and cleaved-caspase 3 staining in mouse carotid artery**s** subjected to disturbed flow. The negative control shows a normal mouse carotid artery without TUNEL staining, showing green autofluorescence only (mainly elastin). (B) Immunofluorescence and immunohistochemistry of cleaved-caspase 3/CD31.

Supplementary Table I: Targeted genes and their accession number

Gene symbol	Gene name	mRNA Accession number	Forward sequence (5'-3')	Reverse Sequence (5'-3')
Actb	Beta-Actin	NM_007393.5	GTCGAGTCGCGTCCACC	GTCATCCATGGCGAACTGGT
Bax	BCL2-Associated X Protein	NM_007527.3	TGCTAGCAAACTGGTGCTCA	GGCCTTCCCAGCCACCC
Bcl2	B-Cell CLL/Lymphoma 2	NM_009741.5	GACTGAGTACCTGAACCGGC	AGTTCCACAAAGGCATCCCAG
Col1a1	Collagen, Type I, Alpha 1	NM_007742.4	TGACTGTCCCACGTAAGCAC	GAGGGCCATAGCTGAACTGA
Col3a1	Collagen, Type III, Alpha 1	NM_009930.2	GAAAGAGGATCTGAGGGCTCG	GGGTGAAAAGCCACCAGACT
Cxcl1	Chemokine (C-X-C Motif) Ligand 1	NM_008176.3	ACCGAAGTCATAGCCACACTC	CTCCGTTACTTGGGGACACC
Cxcl2	Chemokine (C-X-C Motif) Ligand 2	NM_009140.2	TGAACAAAGGCAAGGCTAACTG	CAGGTACGATCCAGGCTTCC
Cxcl5	Chemokine (C-X-C Motif) Ligand 5	NM_009141.3	TGCCCTACGGTGGAAGTCAT	AGCTTTCTTTTTGTCACTGCCC
Esel	Selectin E	NM_011345.2	CATCCTGCAGTGGTCATGGT	GCAAGTCACAGCTTGCTCAC
Has1	Hyaluronan synthase 1	NM_008215.2	TACGTGCAGGTCTGTGACTC	CATCCAACACTCGCACAAGC
Has2	Hyaluronan synthase 2	NM_008216.3	GGCCGGTCGTCTCAAATTCA	ACAATGCATCTTGTTCAGCTCC
Hyal1	Hyaluronidase-1	NM_008317.4	CTTCAGTCCTGAGGTTTCCCC	TGAATGGCCGGTTGGATACC
Hyal 2	Hyaluronidase-2	NM_010489.2	GGCTTGGTTGGTACCAGGAT	GGTAGCAGCTCAGGAACTCG
Icam-1	Intercellular Adhesion Molecule 1	NM_010493.2	TCCGCTGTGCTTTGAGAACT	TCCGGAAACGAATACACGGT
Vcam-1	Vascular Cell Adhesion Molecule 1	NM_011693.3	TATGTCAACGTTGCCCCCAA	CAGGACTGCCCTCCTCTAGT
Vcan	Versican	NM_001081249.1	CAGCTCTGTCCCGCACTC	TCTTGTCCTTGAAAGGCGGC

Supplementary Table II: Comparison between carotid thrombus occlusion between ApoE-/- mice and ApoE-/-TLR2-/- mice

Condition	Thrombus occurrence		p
	ApoE-/- (n=30)	ApoE-/-TLR2-/- (n=39)	
CC +1h	7 (44%)	8 (28%)	<0.05
CC +6h	6 (42%)	1 (9%)	<0.05

	Thrombus occurrence		p	
		%	to sham	to NC
Sham	0/12	0		ns
NC	2/28	7	ns	
CC	25/78	32	<0.05	<0.01

Plaque Erosion

New Insights From the Road Less Travelled

Jacob F. Bentzon, Erling Falk

The exploration of the steps that lead to coronary thrombi needs another chapter. Decades ago, it was found that the majority (≈3 of 4) of lesions underlying lethal thrombi featured a necrotic core into which blood had entered through a severed fibrous cap.[1] Sometimes, bits of core material were embedded in the thrombus linking cap rupture and thrombosis closely in time. Like watching a crashed car or a broken plate, it took modest imagination to understand what must have happened. A thin fibrous cap had ruptured, ripping open the lesion, and exposing the thrombogenic core to the hemostatic system. The lack of a credible alternative mechanism that could explain the observed has made it less of a problem that re-enactment of plaque rupture in model systems or formal proof for the sequence of events in humans have been difficult to achieve.

Article, see p 31

For the remainder of thrombi that are not formed on ruptured plaques, it is a completely different game. These cases give few signs away about what caused them. Endothelial cells (ECs) at the plaque-thrombus interface are generally absent, leading to the term plaque erosion, and macrophages are rarely conspicuous.[2] More notably, neutrophils are often present.[3] But, autopsies cannot tell for sure whether the missing endothelium and neutrophil accumulation were the cause or result of thrombosis. This is not an academic question. EC sloughing and neutrophil invasion occur secondarily to stasis-induced venous thrombosis,[4] and thrombi precipitated by plaque rupture can produce the appearance of plaque erosion in neighboring segments.[2] The idea that erosions are preceded by plaques deprived of large regions of its endothelial lining may thus be far too simple. Rather, processes of EC loss, neutrophil recruitment, and thrombosis may occur simultaneously facilitating growth of thrombus across an erosion-prone lesion surface.

This is part of the lesson that can be learnt from the work of Franck et al[5] in the present issue of *Circulation Research*. In a murine model system that featured components associated with human plaque erosion, they describe a mechanism by which a hyaluronan-rich subendothelial matrix, disturbed blood flow, and neutrophils co-operate to drive endothelial denudation and arterial thrombosis.

Whereas lesions producing thrombi by rupture are invariably fibroatheromas with thin caps, no distinct set of histological features have been identified for the precursors of erosions. They appear as a mixed bag of pathological intimal thickenings and fibroatheromas, with variable degrees of superficial inflammation.[1] Yet one common theme may be the presence of tissues rich in smooth muscle cells and glycosaminoglycans, including hyaluronan, at the plaque-thrombus interface.[6] Hyaluronan is an anionic, nonsulfated extracellular matrix glycosaminoglycan with important structural and signaling properties in multiple organisms and tissues. Its water-retaining properties make it an important constituent of articular cartilage and cosmetic dermal fillers, and fragments of hyaluronan, which is also present in the coat of certain bacteria, signal through Toll-like receptors (TLRs), including TLR2, to facilitate inflammation.[7]

Franck et al[5] show that eroded carotid lesions in humans, as well as nonthrombotic lesions with many apoptotic luminal ECs, have accumulation of superficial neutrophils. This extends their previous work that such lesions are characterized by superficial hyaluronan accumulation and that hyaluronan in vitro signals through TLR2 to activate ECs leading to expression of neutrophil-recruiting chemokines and adhesion molecules.[8]

To create vessels with hyaluronan-rich subendothelial matrix, Franck et al[5] allowed electric injury of murine carotid arteries to heal with formation of smooth muscle cell–rich neointima and regenerated ECs. Subsequently, the healed segment was exposed to disturbed blood flow by the application of a constrictive perivascular cuff. The link between flow patterns and risk of erosion has not been well worked out in humans, but disturbed flow is common in severely atherosclerotic arteries. Because an eroding lesion provides a subtler thrombogenic stimulus than rupture, it makes sense that the other components of the triad of Virchow (flow disturbance and systemic thrombotic propensity) could be particularly important in this setting. Moreover, disturbed blood flow increases endothelial TLR2 expression and apoptosis, thereby triggering the proposed hyaluronan–TLR2–neutrophil axis.[9] With these 2 arterial insults in place, neutrophil accumulation, EC apoptosis, and mural thrombosis resulted (Figure).

Although we cannot be sure that the thrombotic mechanism in this cuffed neointima model replicates the one in human plaque erosion, it copies several components, and importantly, it offers opportunities to establish cause–effect relationships and directionality among them. From the

From the Experimental Pathology of Atherosclerosis, Centro Nacional de Investigaciones Cardiovasculares Carlos III, Madrid, Spain (J.F.B.); and Department of Clinical Medicine, Aarhus University, Denmark (J.F.B., E.F.).

Correspondence to Jacob F. Bentzon, MD, PhD, Experimental Pathology of Atherosclerosis, Centro Nacional de Investigaciones Cardiovasculares Carlos III, Melchor Fernández Almagro 3, 28029 Madrid, Spain. E-mail jfbentzon@cnic.es

(*Circ Res*. 2017;121:8-10.
DOI: 10.1161/CIRCRESAHA.117.311218.)

***Circulation Research* is available at http://circres.ahajournals.org**
DOI: 10.1161/CIRCRESAHA.117.311218

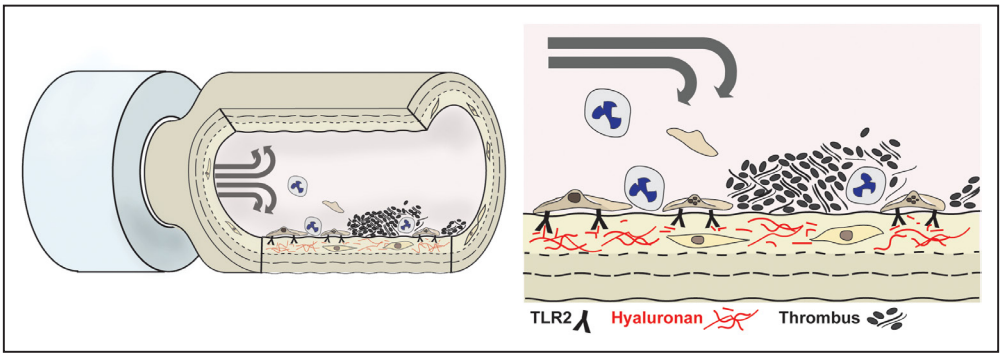

Figure. Schematic of the cuffed neointima model and the proposed thrombotic mechanism. Toll-like receptor 2 (TLR2) signaling, possibly evoked by hyaluronan fragments in the subendothelial matrix, together with disturbed blood flow leads to neutrophil recruitment, endothelial cell apoptosis/sloughing, and thrombus formation.

experiments by Franck et al,[5] we learn that TLR2 signaling is upstream of neutrophil accumulation, which in turn is important for EC loss and thrombosis.[5] The relatively restricted thrombus formation seen in the model may be expected. In our own experience, mechanical rupture of advanced lesions in the mouse carotid bifurcation also rarely lead to more than a small mural thrombus.[10]

The cuffed neointima model is related to and may shed light over the thrombosis mechanism in 2 previously published animal models. Femoral artery stenosis in rabbits induces downstream neointima and thrombus, possibly by similar mechanisms.[11] Carotid tandem stenosis in hyperlipidemic mice has been introduced as a model of plaque rupture, but it is plausible that the thrombotic mechanism may include additional mechanisms.[12]

The interesting work of Franck et al[5] is from a road less travelled by in atherosclerosis research. As the authors rightly note, there is a scarcity of investigation into plaque erosion, which is completely out of proportion with the importance of the problem. Perhaps, it is partly the lack of a relevant model system that has discouraged more researchers from delving into the subject. If that is the case, the cuffed neointima model may inspire others to take on the problem.

Going forward, the established model may offer possibilities to test the causal role of other determinants of erosion proneness in the arterial wall or circulating cells, such as additional matrix components, secreted pro- or antithrombotic factors, and the role of EC phenotype. Previous studies have indicated that injured arteries heal with dysfunctional ECs.[13] Could this contribute to the thrombosis proneness of the cuffed neointima? Is EC senescence resulting from decades of increased EC turnover over atherosclerotic lesions important? Can it be ameliorated?

In a broader perspective, it would be interesting to explore whether the thrombotic mechanism described here has a facilitating role in cases where it is not itself sufficient to precipitate thrombosis. Not all plaque ruptures cause clinical symptoms and even fewer lasting damage or death. Others heal silently with only mural or transient thrombus. Probably, rheological forces and systemic thrombotic propensity are important factors, but one may also speculate that the vulnerability of the neighboring plaque surface for neutrophil-driven endothelial denudation could be a determining factor between the different outcomes. The often protracted development of thrombus and the presence of neutrophils in the plaque-thrombus interface of ruptured plaques lend some support to this idea.[3,14]

Clinical studies using intravascular imaging with optical coherence tomography to detect plaque rupture have found that rupture is the most frequent substrate of ST-segment–elevation myocardial infarction, whereas non–ST-segment–elevation myocardial infarction often develops without optical coherence tomography–detectable rupture.[15] Recent decline in age-adjusted incidence of acute coronary syndrome has been particularly clear for ST-segment–elevation myocardial infarction.[15] These observations indicate that what has been achieved to date in primary and secondary preventions of acute coronary syndrome has been especially effective in counteracting plaque ruptures. It also suggests that the erosion-prone lesion is the next frontier in combating clinical complications from coronary atherosclerosis. Such an endeavor is best helped by a clear understanding of the mechanisms underlying thrombosis with plaque erosion.

Sources of Funding

J.F.B. is supported by research grants from the Danish Council for Independent Research (Sapere Aude II, 4004-00459B) and the Ministerio de Economía, Industria y Competitividad (MEIC; Programa RETOS Estatal de I+D+i Orientada a los Retos de la Sociedad, SAF2016-75580-R) with cofunding by Fondo Europeo de Desarrollo Regional (FEDER). The CNIC is supported by MEIC and the Pro CNIC Foundation, and is a Severo Ochoa Center of Excellence (MINECO award SEV-2015-0505).

Disclosures

None.

References

1. Bentzon JF, Otsuka F, Virmani R, Falk E. Mechanisms of plaque formation and rupture. *Circ Res*. 2014;114:1852–1866.
2. Virmani R, Kolodgie FD, Burke AP, Farb A, Schwartz SM. Lessons from sudden coronary death: a comprehensive morphological classification scheme for atherosclerotic lesions. *Arterioscler Thromb Vasc Biol*. 2000;20:1262–1275.
3. Naruko T, Ueda M, Haze K, van der Wal AC, van der Loos CM, Itoh A, Komatsu R, Ikura Y, Ogami M, Shimada Y, Ehara S, Yoshiyama M, Takeuchi K, Yoshikawa J, Becker AE. Neutrophil infiltration of culprit lesions in acute coronary syndromes. *Circulation*. 2002;106:2894–2900.
4. Moaveni DK, Lynch EM, Luke C, Sood V, Upchurch GR, Wakefield TW, Henke PK. Experimental post thrombosis vein wall re-endothelialization is modulated by low molecular weight heparin. *J Vasc Surg*. 2008;47:616–624. doi: 10.1016/j.jvs.2007.11.040.

5. Franck G, Mawson T, Sausen G, et al. Flow perturbation mediates neutrophil recruitment and potentiates endothelial injury via TLR2 in mice: implications for superficial erosion. *Circ Res*. 2017;121:31–42. doi: 10.1161/CIRCRESAHA.117.310694.
6. Kolodgie FD, Burke AP, Farb A, Weber DK, Kutys R, Wight TN, Virmani R. Differential accumulation of proteoglycans and hyaluronan in culprit lesions: insights into plaque erosion. *Arterioscler Thromb Vasc Biol*. 2002;22:1642–1648.
7. Jiang D, Liang J, Noble PW. Hyaluronan as an immune regulator in human diseases. *Physiol Rev*. 2011;91:221–264. doi: 10.1152/physrev.00052.2009.
8. Quillard T, Araújo HA, Franck G, Shvartz E, Sukhova G, Libby P. TLR2 and neutrophils potentiate endothelial stress, apoptosis and detachment: implications for superficial erosion. *Eur Heart J*. 2015;36:1394–1404. doi: 10.1093/eurheartj/ehv044.
9. Mullick AE, Soldau K, Kiosses WB, Bell TA 3rd, Tobias PS, Curtiss LK. Increased endothelial expression of Toll-like receptor 2 at sites of disturbed blood flow exacerbates early atherogenic events. *J Exp Med*. 2008;205:373–383. doi: 10.1084/jem.20071096.
10. Bentzon JF, Sondergaard CS, Kassem M, Falk E. Smooth muscle cells healing atherosclerotic plaque disruptions are of local, not blood, origin in apolipoprotein E knockout mice. *Circulation*. 2007;116:2053–2061. doi: 10.1161/CIRCULATIONAHA.107.722355.
11. Sumi T, Yamashita A, Matsuda S, Goto S, Nishihira K, Furukoji E, Sugimura H, Kawahara H, Imamura T, Kitamura K, Tamura S, Asada Y. Disturbed blood flow induces erosive injury to smooth muscle cell-rich neointima and promotes thrombus formation in rabbit femoral arteries. *J Thromb Haemost*. 2010;8:1394–1402. doi: 10.1111/j.1538-7836.2010.03843.x.
12. Chen YC, Bui AV, Diesch J, Manasseh R, Hausding C, Rivera J, Haviv I, Agrotis A, Htun NM, Jowett J, Hagemeyer CE, Hannan RD, Bobik A, Peter K. A novel mouse model of atherosclerotic plaque instability for drug testing and mechanistic/therapeutic discoveries using gene and microRNA expression profiling. *Circ Res*. 2013;113:252–265. doi: 10.1161/CIRCRESAHA.113.301562.
13. Vanhoutte PM, Shimokawa H, Feletou M, Tang EH. Endothelial dysfunction and vascular disease—a 30th anniversary update. *Acta Physiol (Oxf)*. 2017;219:22–96. doi: 10.1111/apha.12646.
14. Kramer MC, Rittersma SZ, de Winter RJ, Ladich ER, Fowler DR, Liang YH, Kutys R, Carter-Monroe N, Kolodgie FD, van der Wal AC, Virmani R. Relationship of thrombus healing to underlying plaque morphology in sudden coronary death. *J Am Coll Cardiol*. 2010;55:122–132. doi: 10.1016/j.jacc.2009.09.007.
15. Pasterkamp G, den Ruijter HM, Libby P. Temporal shifts in clinical presentation and underlying mechanisms of atherosclerotic disease. *Nat Rev Cardiol*. 2017;14:21–29. doi: 10.1038/nrcardio.2016.166.

KEY WORDS: Editorials ■ atherosclerosis ■ endothelial cells ■ thrombosis ■ Toll-like receptors

Circulation Research
JOURNAL OF THE AMERICAN HEART ASSOCIATION

Plaque Erosion: New Insights From the Road Less Travelled

Jacob F. Bentzon and Erling Falk

Circ Res. 2017;121:8-10
doi: 10.1161/CIRCRESAHA.117.311218
Circulation Research is published by the American Heart Association, 7272 Greenville Avenue, Dallas, TX 75231

Print ISSN: 0009-7330. Online ISSN: 1524-4571